AN ABSTRACT OF THE DISSERATION OF

Taehyeong Kim for the degree of Doctor of Philosophy in Chemistry presented on November 3, 2011

Title: Organic-solvent Resistant Ultrafiltration and Nanofiltration Membrane Modules for Separation and Purification of Nanoparticles

Abstract approved:

_____

Vincent T. Remcho

The intriguing size- and shape dependent properties of nanoparticles have garnered recent attention in many science and engineering areas. When the particle size is in the nanometer size range, the material exhibits very different properties such as surface plasmon resonance (of gold nanoparticles) and superparamagnetism (of iron oxide nanoparticles). The size-dependent properties of quantum dots have made them useful as UV-Vis-NIR sensors and in telecommunications applications. However, the separation and purification of nanoparticles are still challenging due to their size, insolubility in many solvents, and irreversible adsorption to other materials. Membrane filtration is widely used to separate nano-sized biological materials such as

proteins, viruses, DNA and RNA. This dissertation presents novel approaches to the use of ultrafiltration and nanofiltration membranes for nanoparticle separation and purification using dead-end and cross-flow filtration techniques.

Purification of phosphine-stabilized Au_{11} ($Au_{11}(PPh_3)_8Cl_3$, M.W. 4371, d_{core}=0.8 nm), produced in a microreactor without recrystallization, was achieved using nanofiltration membranes. The ceramic and polymer nanofiltration membranes were able to purify the Au_{11} with rejection values higher than 90%. A novel continuous nanofiltration system design was applied and characterized. The continuous synthesis process, coupled with continuous nanofiltration, resulted in a significant reduction in synthesis time while producing higher yield than could be achieved in batch experiments. The diafiltration system was applied towards isolation of Au_{11}, and results were presented that indicate increased yield and enhanced product purity.

Organic-solvent resistant nanofiltration and ultrafiltration membranes were applied for purification and size-based separation of lead sulfide nanoparticles and gold nanoparticles that were initially synthesized with a 2-8nm size distribution. The nanofiltration membranes achieved rejection values greater than 95% for each of the nanoparticle samples and retained most of the nanoparticles on the membranes. The nanofiltration membranes also exhibited high permeability, which translates to a reduced purification time. Ultrafiltration membranes were screened and successfully applied to the size fractionation of lead sulfide nanoparticles and gold nanoparticles.

A templated silsesquioxane (ssq) membrane was synthesized within the pore space of an alumina support membrane and used for the separation and purification of nano-sized materials such as nanoparticles and macromolecules. The ssq membrane was fabricated by polycondensation of a silsesquioxane monomer solution in the presence of a surfactant within the macroporous space of an Anodisc alumina membrane (Whatman, CO. Ltd, Maidstone, UK). The novel ssq membranes were successfully applied for size exclusion separations of organic soluble 5-8 nm gold nanoparticles (protected with dodecanethiol). A ssq membrane also proved useful for the separation of biological macromolecules such as bovine serum albumin and myoglobin.

Organic-solvent Resistant Ultrafiltration and Nanofiltration Membranes Modules for Separation and Purification of Nanoparticles

by

Taehyeong Kim

A DISSERTATION

Submitted to

Oregon State University

in partial fulfillment of

the requirements for the

degree of

Doctor of Philosophy

Presented November 3, 2011

Commencement June 2012

Doctor of Philosophy dissertation of Taehyeong Kim

presented on November 3, 2011

APPROVED:

_____

Major Professor, representing Chemistry

_____

Chair of the Department of Chemistry

_____

Dean of the Graduate School

I understand that my dissertation will become part of the permanent collection of Oregon State University libraries. My signature below authorizes release of my dissertation to any reader upon request.

_____

Taehyeong Kim, Author

ACKNOWLEDGEMENTS

Graduate school is a long trail without a map and a GPS, but there were people who showed me the direction. First of all, I would like to thank my advisor, Dr. Vincent T. Remcho for his support and guidance through this experience. I really appreciate the opportunity that he has provided me.

I warmly thank Dr. David Cann, Dr. Chih-hung Chang, Dr. Douglas Keszler and Dr. Neal Sleszynski for their advice and participation as my committee members.

Many thanks for Dana and Jack. Their help and advice for this project made my work possible. I would also like to express my thanks to my previous and current lab members: Adeniyi, Beth, Brian, Carlos, Chris, Corey, Esha, Jintana (Dao), Myra, Nataliia, Ryan, Saki, Yolanda, YY, Kelsie and Zoe. They all gave me good advice, or helped me in some way at some points

I appreciate to thank my collaborators, Dr. Hyung Dae Jin and Dr. Lallie McKenzie for discussing the gold nanoparticle synthesis and characterization date. I wish to thank Teresa and Dr. Liu for their help and suggestions in electron microscopy. Milton Harris Graduate fellowship for financial assistance, Department of Chemistry and College of Science at Oregon State University for travel fellowship are also thankful.

I would like to appreciate my parents for their supporting and prayer, and my brother for his comfort and advice. Finally, my wife, HyunJung, I always appreciates your generosity and motivation. You and our baby, Liam, are wonderful gift for me.

TABLE OF CONTENTS

Page

TABLE OF CONTENTS (Continued)

Page

TABLE OF CONTENTS (Continued)

Page

TABLE OF CONTENTS (Continued)

Page

LIST OF FIGURES

Figure Page

LIST OF FIGURES (continued)

Figure Page

LIST OF FIGURES (Continued)

Figure Page

LIST of TABLES

Table Page

Chapter 1 An introduction to the separation and purification of nanoparticles

Nanotechnology has become very popular with the biological and chemical communities of the twenty-first century. Nanotechnology funding has increased more than four-fold from $494 million in 2001 to $ 2.13 billion in 2012.[1] Based on the terminology “nano” in the metric system, one nanometer is equal to one-billionth of a meter. A nanometer is one million times smaller than single human hair (100 μm) and approximately ten hydrogen atoms across. Materials larger than 1 μm have similar properties to bulk materials, but nano-sized materials have distinctly different properties. For example, gold nanoparticles have a red color that arises from surface-plasmon resonance (SPR), that is, the collective oscillation of the electrons in the conduction band of a gold nanoparticle. Quantum dots (QD) are high fluorescence nanoparticles (NPs), and their λmax wavelength of emission and first excitation are dependent on their size. Nano-sized crystals have a lower melting point than bulk materials. The difference can be as large as 1000˚C because the surface contains the major portion of the total number of atoms or ions; thus, their thermal stability is affected by the surface energy. The properties of nanoparticles are controlled by their size and shape.[2]

Unique approaches to the synthesis of nanoparticles have been introduced, such as the chemical reduction of inorganic precursors and the hot-injection method. The size and shape of nanoparticles have been controlled by the stoichiometry ratio, the reaction

time, and the temperature, which ideally generates monodisperse nanoparticles. However, the major difficulty in the synthesis of nanoparticles is controlling their size and thereby their size-dependent properties. If the nanoparticles are monodisperse, they are a single-size and their properties are easily defined; however, if the nanoparticles are produced by attrition, they are polydisperse and their properties over a broad range when compared to single-size nanoparticles. The purification and separation of synthetic nanoparticles is important for reducing further reactions by Ostwald ripening [3], removing interfering starting materials and byproducts that have similar chemical properties, and obtaining a narrow particle size distribution. The purification and separation of nanoparticles is also a challenge because nanoparticles do not typically dissolve in solution, but instead disperse in the solvent: each individual nanoparticle exists as a single particle or crystal in the liquid system.

Approaches to separation and purification of nanoparticles are based on methods routinely applied to inorganic and organic materials and macromolecules, and maybe selective for material property or size. Nanoparticles often consist of an inorganic (metal) core decorated with organic ligands in the 1 k – 1000 kD molecular weight range. Purification and separation strategies for these molecules capitalize on differences in their chemical and physical properties, such as polarity, solubility, and molecular weight, to isolate them by solvent washing, liquid-liquid extraction, and centrifugation. Due to the size differences of nanoparticles and their byproducts, it is also possible to use membrane filtration, chromatography, and field-flow fractionation to separate them. [4,5] To characterize their sizes and optical properties, electron

microscopy, dynamic light scattering, and UV-Vis-NIR spectroscopy are widely used. The first half of this chapter introduces these techniques and focuses on their application to nanoparticles.

Mesoporous materials with pore diameters between 2 and 50 nm are also drawing attention as nanomaterials. The nanosized pores on the surface of and inside these materials are generally intended to create a complex structure with high surface area, high strength, low dielectric constant, low thermal conductivity, and mechanical flexibility. [6] Silsesquioxane, an organic-inorganic hybrid material, can be utilized as a membrane medium for fractionation of nanoparticles by entrapping it within the mesopores of an alumina membrane. The last half of this chapter introduces this supported silsesquioxane membrane.

1.1 The purification and separation of nanoparticles

1.1.1 Solvent washing, liquid-liquid extraction, and size-selective precipitation

Differences in polarity between the various target nanoparticles and their byproducts, such as extra precursors, ligands, and other byproducts, can be exploited to achieve solubility-based separation using methods such as solvent washing, liquid-liquid extraction, and size-selective precipitation. To optimize the solvent system and the results of the repetitive washing steps, a large amount of time and solvent is needed.[7]

Loss of sample is possible with solvent washing. After the purification process, water–soluble nanoparticles must be separated from residual salts using other processes.

1.1.2 Centrifugation and density-gradient ultracentrifugation

A nanoparticle solution is an even dispersion of each type of nanoparticle in the solvent. The separation of flocculates and supernatants by centrifugation produces a precipitate enriched with the high molecular weight nanoparticles. Light dissolved byproducts and tiny nanoparticles remain in the suspension and are removed with the flocculate. The centrifugation method has the advantage of being simple and less expensive than many other options [8], but byproducts frequently remain in the flocculate necessitating several solvent washes and dialyses.

Recently, a density-gradient ultracentrifugation method has been applied to the separation of different sized nanoparticles. [9–12] Concentrated nanoparticle mixtures are stacked on multilayer step-density gradient media rather than into the an empty centrifugation tube. The water/media mixture controls the media density, and moves the media relative to the nanoparticles. The gradient-density step, size and centrifugation force and time, enable the retention of large size nanoparticles in the media.[9] The particle size differences affect the migration of nanoparticles to the bottom of the test tube. (Figure 1.1) Gold nanoparticles in the 20-200 nm size range [11] and nanorods with different aspect ratios [12] have successfully been separated by multilayer gradient centrifugation. However, the amount of sample that can be separated in one test tube is limited, and several density layer combinations and centrifugation times and speeds are necessary to optimize the analysis.

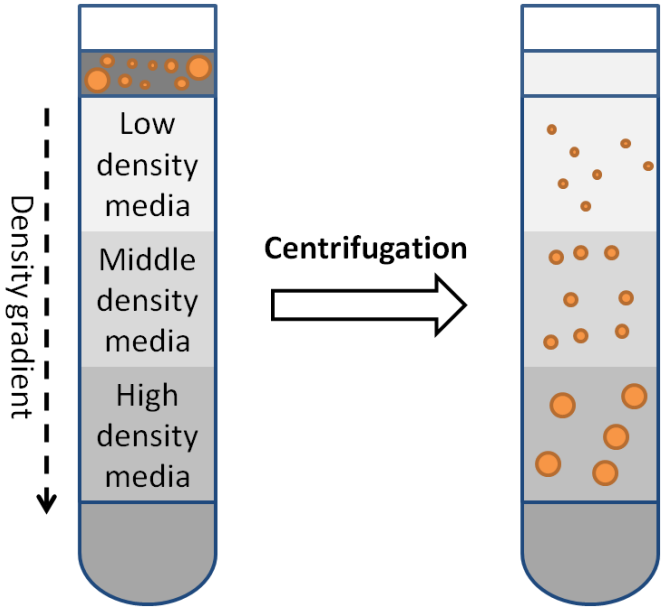

Figure 1.1 The separation of different sized nanoparticle mixtures in a multilayer density gradient by ultracentrifugation. The centrifugation tube is filled with the media mixture at different gradient ratios.

1.1.3 Membrane filtration

Membrane filtration has been used to separate or concentrate a desired products via careful selection of the membrane pore size. Membrane filtration has been used extensively in biological areas (such as the food industry) for the separation of macromolecules. [13] Ultrafiltration and nanofiltration membranes mostly cover the nanometer range. The 1996 IUPAC-nomenclature defines nanofiltration as the process of rejecting particles and dissolved molecules smaller than 2 nm and defines ultrafiltration as lying between 2 nm and 0.1 µm.[14] Membrane-based filtration using media of a stated pore size has the following benefits: estimation of size-exclusion performance, easy scale-up by expanding the membrane area, convenient connections between processing tools such as reactors and analysis devices, and a greener process

that saves solvent during the purification and separation steps. Filtration processes are defined as dead-end or cross-flow by the solution stream direction. A dead-end flow filtration has the flow and pressure directed at the membrane. In a cross-flow filtration, the flow direction is parallel to the membrane surface, and the pressure is perpendicular to the surface. This set-up has proved effective in reducing the clogging of membrane pores and is a scalable method that allows continuous-flow operation. (Figure 1.2)

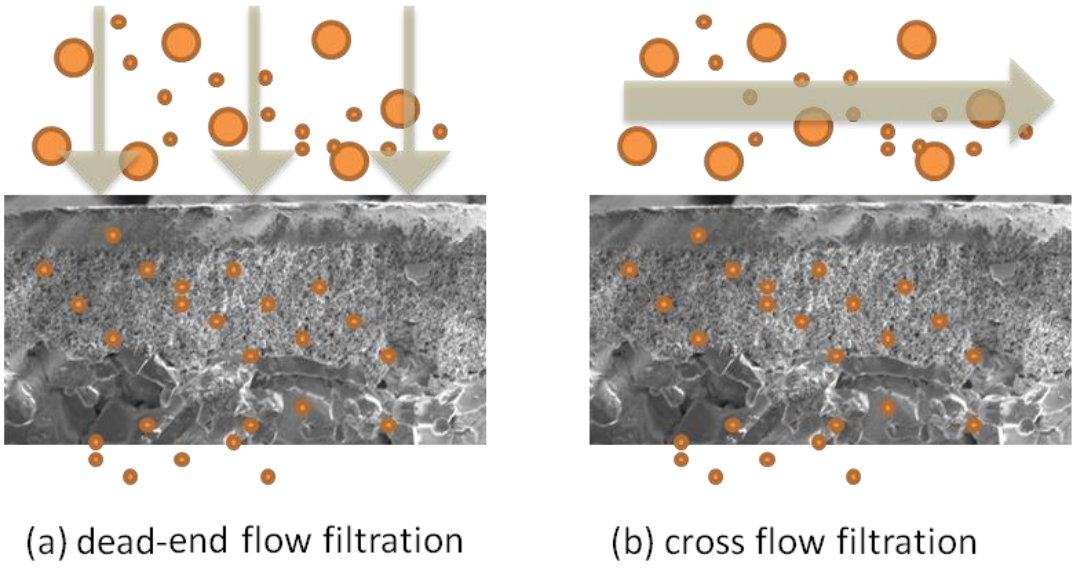

Figure 1.2 Membrane filtration designs; (a) dead-end flow filtration, (b) cross-flow filtration.

Ultrafiltration membranes have been used for size separation of Fe_2O_3 nanoparticles[15], gold nanoparticles[16,17], silver nanoparticles[18] and fullerene nanoparticles[19] by dead-end or cross-flow filtration. A series of variously sized gold

nanoparticles was separated efficiently using the diafiltration method [17] and even a nanofiber was separated from a mixture of nanoparticles and their nanofibers by cross-flow filtration. [20] Compared to ultracentrifugation, it has been reported that the ultrafiltration method causes less aggregation of nanoparticles and has more concentration efficiency. [18] However, membrane fouling from the build-up of nanoparticles means that the membrane needs to be cleaned or exchanged regularly to maintain performance. The irregular pore sizes of tortuous membranes and the stated pore size based on the molecular weight cut-off can cause unexpected results, such as decreased permeation and non-filtration. Polymeric membranes have less compatibility with various organic solvents, which can cause swelling that changes the pore size.[21] Chapters two and three will discuss the filtration of nanoparticles using organic solvent-resistant nanofiltration and ultrafiltration membranes.

1.1.4 Chromatography

The fine fractionation of chemical or biological mixtures has been developed into a chromatography technique. To analyze and characterize the size of macromolecules, size-exclusion chromatography (SEC) is most commonly used. Particles in the range of a few- to a few hundred nanometers can be fractionated based on residence time differences in an SEC column packed with porous silica or other microporous particles. (Figure 1.3)

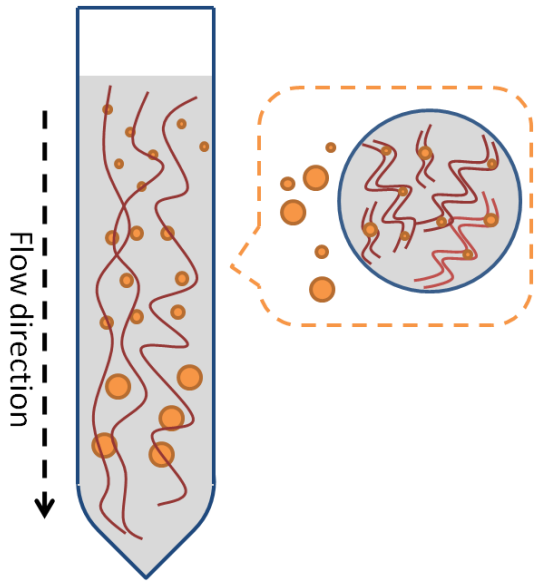

Figure 1.3 A scheme of size exclusion chromatography. Large nanoparticles were excluded, but smaller nanoparticles were retained or had longer migration times in the microporous column material.

SEC is an ideal solution for separation of nanomaterials. Nanoparticles larger than the pore-size of the packing material are excluded and show no retention, while smaller nanoparticles are able to penetrate or permeate into the pore space of the packing material and are retained on the column in decreasing order of size (Figure 1.3). SEC has been shown to be a good size-based separation method for carbon nanotubes [22–25], CdSe nanocrystals [26], silica nanoparticles [27], and gold nanoparticles [28–34]. Recently, the packing material was extended to monolithic capillary columns [27], and the separation of ultrasmall nanoparticles (<2 nm) by SEC is now feasible [34]. High performance liquid chromatography (HPLC) with reverse phase columns [35–39] was used to separate organic-soluble gold nanoparticles using diode array detection (DAD)

or cyclic voltammetric detection. SEC as an HPLC technique would be an efficient and accurate method for size fractionation of nanoparticles. However, the sample capacity of the column is limited to a very small amount (micrograms) and the irreversible adsorption of nanoparticles onto the stationary phase lowered the recovery and the yield. The low resolution of the SEC makes it a challenge to separate different sized nanoparticles at high resolution using this approach.

1.1.5 Electrophoresis

Gel electrophoresis is the most common method for the separation of biological macromolecules such as protein, DNA and RNA. Analytes can be sorted by size and charge in a gel media using electrophoresis. Gold and silver nanoparticles having a charged polymer layer were separated by agarose gel electrophoresis, [40] and single-walled carbon nanotubes derived from arc-discharge soot were purified on the preparative scale [25]. Compared to other separation methods, gel electrophoresis can run multiple samples in parallel on the same media, and the migration of standards and mixtures can be compared. However, nanoparticles need a charged passivative layer to migrate in a gel. Post-processes are required for the characterization of nanoparticles.

Capillary electrophoresis (CE) is a separation tool that uses differences in the electrophoretic mobilities of particles in an electric field to separate them. Compared to charged macromolecules such as viruses and proteins, the charge densities and radii of nanoparticles are suitable for successful CE separation. The separation of gold and silver nanoparticles and CNT, using CE was reviewed by Liu and Valcarel. [4,41]. CE is an attractive method due to the low consumption of samples and reagents in the

separation process, the rapid separation times, and the high efficiency of the long narrow capillary. However, as in the chromatography techniques, only a small amount sample can be subjected to CE. This technique is limited to charged particles, and pre-conditioning of non-water soluble particles is necessary.

1.1.6 Field-flow fraction (FFF)

Flow-assisted hydrodynamic separation techniques are able to separate nano-sized macromolecules and particles. The even channel flow (cross flow) and an external field flow (in a downward direction) generate different displacements for different-sized nanoparticles in the fluid stream. The sample mixture migrates toward one side of the channel by virtue of the channel flow, is lifted by diffusion and hydrodynamic forces, and sinks under the influence of the downward flow. Thus, the particle mixture distributes in the vertical direction; and particles are separated into zones of differing transport velocity. (Figure 1.4) The outlet flow from the FFF system can be characterized using in-line detectors such as UV-Vis, fluorescence and dynamic light scattering (DLS). Hofmann et al. reviewed various field-flow fraction techniques for nanoparticles in complex food and environmental samples. [42] However, the small quantities (in the µg to ng range) of sample, the technique can accommodate, limit size fractionation through FFF.

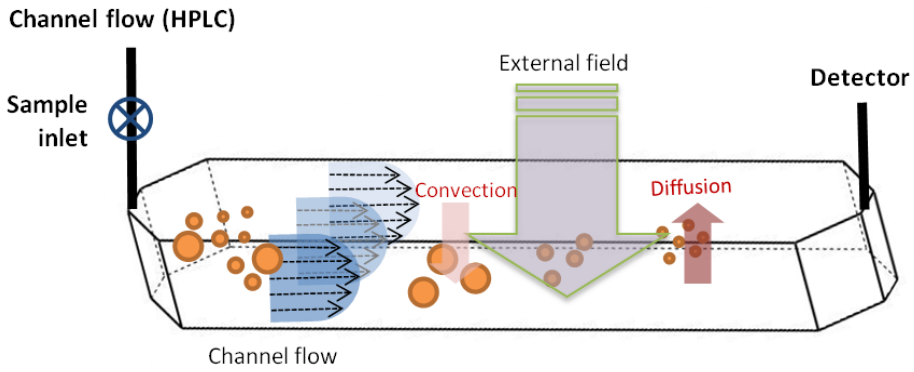

Figure 1.4 A schematic the field flow fraction technique for particle size analysis. The membrane composes the top and bottom side, or only the bottom side of the channel in the case of an external field.

1.2 Characterization methods

1.2.1 Electron microscopy

Transmission electron microscopy (TEM) is the most common technique used to provide precise structural information about a nanoparticle. [43,44] The precise size distribution from TEM results surpasses those of other characterization methods. However, TEM analysis for particle size distribution collection is time intensive.

The limitation of statistical uncertainty also exists because the probed grid area cannot provide the overall particle distribution of a sample. However, the images from other techniques cannot compare to the precise images from TEM. The energy-dispersive X-ray pattern and diffraction pattern of TEM can be useful for determining the atomic

composition and crystal properties, respectively. However, the sample must be isolated for analysis, which is time consuming.

1.2.2 Optical absorbance or fluorescence spectrometry

Nanoparticle solutions are broadly characterized by nanoparticle optical absorbance or fluorescence properties, such as the red and yellow colors of surface plasmon resonance (SPR) absorbance of gold and silver nanoparticles, respectively, and the fluorescence of quantum confinement of quantum dots. [6] Based on Beer's law, the absorbance of gold nanoparticles during SPR is proportional to the concentration of nanoparticles in a unit dispersion; hence, the total quantity of nanoparticles can be calculated if standards can be obtained. [45] The size-dependent optical properties of PbS nanocrystals influence their band gap; the λmax of the first exciton wavelength is related to their size. Absorbance and fluorescence spectra are useful for characterizing nanoparticles and are used for optical applications such as in biosensors and photovoltaic materials; however, the lower sensitivity of optical spectrometry limits the detection of low concentrations of nanoparticles. The aggregation of nanoparticles often causes changes in their spectra, specifically in peak position and peak intensity.

1.2.3 Dynamic light scattering (DLS)

DLS is used to determine the hydrodynamic diameter of nanoparticles in liquids from the differences in the refractive index between the particles and the medium. When the high light absorbance of small nanoparticles reduces their scattering, the detection of

these particles is not practical due to the low signal-to-noise ratio of DLS. The polydispersity of large particles also limits the applicability of DLS.[4]

1.2.4 Mass spectrometry

Mass spectrometry (MS) is used to characterize the mass-to-charge ratio (m/z) of a charged species. The fragmentation patterns of materials during the ionization process provide structural information. The m/z of a nanoparticle and its fragmentation pattern are useful means by which to assay the size of nanoparticles and to characterize the chemical structure of the passivation layer. However, large nanoparticles have m/z values that limit their ability to be characterized by MS. For example, a 5 nm gold nanoparticle has a "molar" mass of 754 kDa given that the density of gold is 19.3 g/cm^3. [5] Mass spectrometry is therefore practical for characterizing and quantifying only smaller nanoparticles (<2 nm).

Purification and separation methods for nanoparticles are developing as fast as nanotechnology. The size-dependent properties of nanoparticles suggest that purification and separation techniques are directly coupled to the synthesis process to minimize the polydispersity that arises from an extended reaction time. Membrane filtration techniques have the advantage of being easily attached to continuous reactors and extending the filtration area to process larger amounts of samples, as in a "nano-factory". In this thesis, the smallest gold nanoparticles from the direct or indirect post-synthetic products were purified using dead-end and cross-flow filtration. In chapters

2 and 3, the ultrafiltration and nanofiltration membranes were applied to the separation of 2-8 nm gold and lead sulfide nanoparticles.

1.3 A silsesquioxane template membrane

Silsesquioxanes, $(RO)_3Si\text{-}R'\text{-}Si(OR)_3$, are a family of hybrid inorganic-organic materials that are prepared via the hydrolysis and condensation of a bissilylated organic precursor. The precursor has an organic group (R') and a tri-alkoxysilyl group ($Si(OR)_3$). The condensation of the precursor allows the formation of periodic mesoporous organosilicas (PMOs). [46] The incorporation of organic groups into the inorganic framework has several distinct advantages over terminally bonded organic groups. Up to 100% of the Si atoms in PMOs are connected to organic groups. [47] This structure of the PMOs yields a material with a high surface area, an ordered pore arrangement, uniform pore size, and good chemical and thermal stability. The homogenous distribution of organic groups in the framework and inside the pore walls of PMOs results in a unique electrical, optical, and chemical space. Therefore, PMOs have been the subject of many theoretical and applied studies, in nanoparticle synthesis, catalysis, low-k-microelectronic packing material production, chromatography, drug delivery, and chemical sensors. [47,48]

The formation of PMOs starts with structure-directing agents (surfactants) that form self-assembled micelles when their concentration (in a given acidic or basic solution) is higher than the critical micelle concentration. On its scaffold of surfactant micelles,

the precursor silsesquioxanes self-assembles into a mesostructured organic-inorganic PMOs, as shown in Figure 1.5. The surfactant templates are removed by solvent extraction or calcination. The reaction can be controlled by various conditions, such as temperature, concentration, precursor, surfactant, pH, aging condition, and template removal. These factors adjust the pore size, pore connectivity, surface functionality, hydrophobicity, and channel orientation. [49]

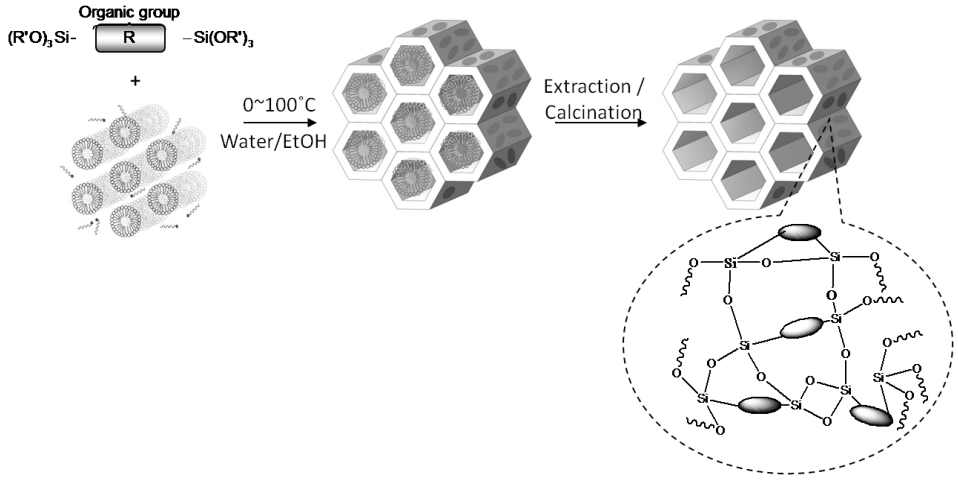

Figure 1.5 PMO synthesis from bridged silsesquioxanes

Thin films of PMOs have been synthesized on a batch scale. [50–52] However, there are inherent drawbacks. The entire synthetic procedure consumes several hours or even days, and the products are irregularly sized powders that require extra processing steps to produce thin films. Self-supporting thin films, made of mesoporous materials with uniform pore structures, have been prepared at solid/liquid or air/water interfaces

using evaporation induced self-assembly (EISA). [53,54] The homogenous precursor and surfactant solutions are prepared in an ethanol/water mixture with the surfactant's concentration being lower than the critical micelle concentration. As the solvent evaporates, the constantly increasing surfactant concentration enables the self-assembly of surfactant micelles. These micelles serve as nuclei to seed the growth and orient the formation of PMOs. Thin films of mesoporous silica composed of two-dimensional nanochannels have been produced. [47,55] The hexagonal silica nanochannels, prepared by the EISA method, are aligned parallel to the substrate's surface.

A method for growing mesoporous silica within an Anodisc alumina membrane (AAM) has also been reported. [56] Instead of a nonporous metal substrate, each pore of the AAM provides a frame in which to grow mesoporous silica. The precursor solution was deposited on the AAM and then drawn through under a vacuum, causing the precursor solution to permeate through the pore space of the AAM. The solvent was then evaporated, which allowed the bundles of mesoporous one-dimensional (1D) silsesquioxane nanochannels (20 to 200 nm) in the pores of the AAM to grow perpendicularly to the membrane's surface. The chemical and thermal resistance of inorganic membranes like AAM can endure the harsh conditions needed for mesoporous silica synthesis, which includes modern acidic or basic solvents and high temperatures. (Figure 1.6) Furthermore, the 60 μm thickness of AAM is attractive for incorporation into microfluidic devices. In another method, AAM was used to support a dual layer microporous/mesoporous silica membrane. The mesoporous silica

sublayer was applied to the AAM by dip-coating. Subsequently, microporous silica was deposited on the mesoporous silicas by spin-coating, which resulted in a highly selective gas-separation membrane. [57] In chapter 4, the aspiration methods were combined to synthesize unique PMOs on an AAM creating a novel membrane. Organic-soluble gold and lead sulfide nanoparticles and proteins were used to verify the filtration performance of the new material.

1.4 References

[1] M. C. Roco, in:, AAAS REPORT XXXVI - RESEARCH AND DEVELOPMENT FY 2012, American Association for the Advancement of Science, 2011.

[2] G. Cao, Nanostructures & Nanomaterials: Synthesis, Properties & Applications, 1st ed., Imperial College Press, 2004.

[3] R. Boistelle, J.P. Astier, J. Cryst. Growth 90 (1988) 14-30.

[4] F.-K. Liu, J. Chromatogr. A 1216 (2009) 9034-9047.

[5] L. Yu, A. Andriola, Talanta 82 (2010) 869-875.

[6] L. Cademartiri, G.A. Ozin, Concepts of Nanochemistry, Wiley-VCH, 2009.

[7] C.B. Murray, D.J. Norris, M.G. Bawendi, J. Am. Chem. Soc. 115 (1993) 8706-8715.

[8] J.P. Novak, C. Nickerson, S. Franzen, D.L. Feldheim, Anal. Chem. 73 (2001) 5758-5761.

[9] X. Sun, S.M. Tabakman, W. Seo, L. Zhang, G. Zhang, S. Sherlock, L. Bai, H. Dai, Angew. Chem. Int. Ed. 48 (2009) 939-942.

[10] L. Bai, X. Ma, J. Liu, X. Sun, D. Zhao, D.G. Evans, J. Am. Chem. Soc. 132 (2010) 2333-2337.

[11] D. Steinigeweg, M. Schütz, M. Salehi, S. Schlücker, Small (2011).

[12] B. Xiong, J. Cheng, Y. Qiao, R. Zhou, Y. He, E.S. Yeung, J. Chromatogr. A 1218 (2011) 3823-3829.

[13] A. Saxena, B.P. Tripathi, M. Kumar, V.K. Shahi, Adv. Colloid Interface Sci. 145 (2009) 1-22.

[14] W. J. Koros, Y. H. Ma, T. Shimidzu, J. Membr. Sci. 120 (1996) 149-159.

[15] Q.-L. Xie, J. Liu, X.-X. Xu, G.-B. Han, H.-P. Xia, X.-M. He, Sep. Purif. Technol. 66 (2009) 148-152.

[16] I. Arnaud, J.-P. Abid, C. Roussel, H.H. Girault, Chem. Commun. (2005) 787.

[17] S.F. Sweeney, G.H. Woehrle, J.E. Hutchison, J. Am. Chem. Soc. 128 (2006) 3190-3197.

[18] J.C. Trefry, J.L. Monahan, K.M. Weaver, A.J. Meyerhoefer, M.M. Markopolous, Z.S. Arnold, D.P. Wooley, I.E. Pavel, J. Am. Chem. Soc. 132 (2010) 10970-10972.

[19] D. Jassby, S.-R. Chae, Z. Hendren, M. Wiesner, J. Colloid Interface Sci. 346 (2010) 296-302.

[20] K.C. Pradel, K. Sohn, J. Huang, Angew. Chem. Int. Ed. 50 (2011) 3412-3416.

[21] P. Vandezande, L.E.M. Gevers, I.F.J. Vankelecom, Chem. Soc. Rev. 37 (2008) 365-405.

[22] B. Zhao, H. Hu, S. Niyogi, M.E. Itkis, M.A. Hamon, P. Bhowmik, M.S. Meier, R.C. Haddon, J. Am. Chem. Soc. 123 (2001) 11673-11677.

[23] S. Niyogi, H. Hu, M.A. Hamon, P. Bhowmik, B. Zhao, S.M. Rozenzhak, J. Chen, M.E. Itkis, M.S. Meier, R.C. Haddon, J. Am. Chem. Soc. 123 (2001) 733-734.

[24] D. Chattopadhyay, S. Lastella, S. Kim, F. Papadimitrakopoulos, J. Am. Chem. Soc. 124 (2002) 728-729.

[25] X. Xu, R. Ray, Y. Gu, H.J. Ploehn, L. Gearheart, K. Raker, W.A. Scrivens, J. Am. Chem. Soc. 126 (2004) 12736-12737.

[26] K.M. Krueger, A.M. Al-Somali, J.C. Falkner, V.L. Colvin, Anal. Chem. 77 (2005) 3511-3515.

[27] K. Sakai-Kato, S. Ota, T. Takeuchi, T. Kawanishi, J. Chromatogr. A 1218 (2011) 5520-5526.

[28] G.-T. Wei, F.-K. Liu, J. Chromatogr. A 836 (1999) 253-260.

[29] G.-T. Wei, F.-K. Liu, C.R.C. Wang, Anal. Chem. 71 (1999) 2085-2091.

[30] A.M. Al-Somali, K.M. Krueger, J.C. Falkner, V.L. Colvin, Anal. Chem. 76 (2004) 5903-5910.

[31] J.P. Wilcoxon, P. Provencio, J. Phys. Chem. B 107 (2003) 12949-12957.

[32] J.P. Wilcoxon, J.E. Martin, P. Provencio, Langmuir 16 (2000) 9912-9920.

[33] H. Tsunoyama, Y. Negishi, T. Tsukuda, J. Am. Chem. Soc. 128 (2006) 6036-6037.

[34] S. Knoppe, J. Boudon, I. Dolamic, A. Dass, T. Bürgi, Anal. Chem. 83 (2011) 5056-5061.

[35] V.L. Jimenez, M.C. Leopold, C. Mazzitelli, J.W. Jorgenson, R.W. Murray, Anal. Chem. 75 (2003) 199-206.

[36] Y. Song, M.L. Heien, V. Jimenez, R.M. Wightman, R.W. Murray, Anal. Chem. 76 (2004) 4911-4919.

[37] Y. Song, V. Jimenez, C. McKinney, R. Donkers, R.W. Murray, Anal. Chem. 75 (2003) 5088-5096.

[38] A. Dass, R. Guo, J.B. Tracy, R. Balasubramanian, A.D. Douglas, R.W. Murray, Langmuir 24 (2008) 310-315.

[39] R.L. Wolfe, R.W. Murray, Anal. Chem. 78 (2006) 1167-1173.

[40] M. Hanauer, S. Pierrat, I. Zins, A. Lotz, C. Sönnichsen, Nano Letters 7 (2007) 2881-2885.

[41] A.I. López-Lorente, B.M. Simonet, M. Valcárcel, TrAC, Trends Anal. Chem. 30 (2011) 58-71.

[42] F. von der Kammer, S. Legros, T. Hofmann, E.H. Larsen, K. Loeschner, TrAC, Trends Anal. Chem. 30 (2011) 425-436.

[43] G.L. Hornyak, S. Peschel, T. Sawitowski, G. Schmid, Micron 29 (1998) 183-190.

[44] W.D. Pyrz, D.J. Buttrey, Langmuir 24 (2008) 11350-11360.

[45] P. Mulvaney, Langmuir 12 (1996) 788-800.

[46] F. Hoffmann, M. Cornelius, J. Morell, M. Fröba, Angew. Chem. Int. Ed. 45 (2006) 3216-3251.

[47] Ö. Dag, C. Yoshina-Ishii, T. Asefa, M.J. MacLachlan, H. Grondey, N. Coombs, G.A. Ozin, Adv. Funct. Mater. 11 (2001) 213-217.

[48] G. Schottner, Chem. Mater. 13 (2001) 3422-3435.

[49] W.J. Hunks, G.A. Ozin, J. Mater. Chem. 15 (2005) 3716-3724.

[50] Y. Lu, R. Ganguli, C.A. Drewien, M.T. Anderson, C.J. Brinker, W. Gong, Y. Guo, H. Soyez, B. Dunn, M.H. Huang, J.I. Zink, Nature 389 (1997) 364-368.

[51] B.D. Hatton, K. Landskron, W. Whitnall, D.D. Perovic, G.A. Ozin, Adv. Funct. Mater. 15 (2005) 823-829.

[52] G.J.A.A. Soler-Illia, P. Innocenzi, Chem. Eur. J. 12 (2006) 4478-4494.

[53] S.S. Park, C.-S. Ha, Chem. Mater. 17 (2005) 3519-3523.

[54] C.J. Brinker, Y. Lu, A. Sellinger, H. Fan, Adv. Mater. 11 (1999) 579-585.

[55] Y. Lu, H. Fan, N. Doke, D.A. Loy, R.A. Assink, D.A. LaVan, C.J. Brinker, J. Am. Chem. Soc. 122 (2000) 5258-5261.

[56] A. Yamaguchi, F. Uejo, T. Yoda, T. Uchida, Y. Tanamura, T. Yamashita, N. Teramae, Nat. Mater. 3 (2004) 337-341.

[57] Y.-B. Jiang, G. Xomeritakis, Z. Chen, D. Dunphy, D.J. Kissel, J.L. Cecchi, C.J. Brinker, J. Am. Chem. Soc. 129 (2007) 15446-15447.

Chapter 2 Purification of Gold Eleven Nanoparticles (Au_{11}) using Nanofiltration Membranes

2.1 Abstract

The purification of phosphine-stabilized Au_{11} ($Au_{11}(PPH_3)_8Cl_3$, M.W. 4371, d_{core}=0.82 nm), produced in a microreactor without recrystallization, was performed using various nanofiltration membranes. An Inopor® nano-membrane (a molecular weight cut-off (MWCO) value of 450 Daltons and a mean pore size of 0.9 nm), and a DuraMem^{TM}500 membrane (MWCO value of 500) were utilized in a dead-end flow filtration scheme and successfully produced a rejection values of 93% and 82%, respectively, for Au_{11} standard solutions. Also developed was a diafiltration method suitable for the purification of post-synthetic Au_{11} by cross-flow filtration. UV-Vis spectroscopic and NMR analyses showed that the ceramic (Inopor® nano) nanofiltration membrane offered a useful ability to purify post-synthetic Au_{11} from byproducts. Transmission electron microscopic (TEM) analysis provided for characterization of the Au_{11}.

2.2 Introduction

Nanofiltration membrane media have become attractive for the separation and purification of mixtures of macromolecules and nanoparticles. Aqueous nanofiltration system has been developed for food production and waterwaste purification process.

[1] However, organic solvent resistant nanofiltration (OSN) membranes have recently been researched and reported in a few applications in pharmaceutical and petrochemical studies. [2–6] Beyond the transport selectivity of the nanofiltration membrane, depending on the molecular weight of the material, an ideal approach might include the application of particle size-exclusion based on the nano-pores. What has been envisioned includes a simple nanoparticle filter that retains nanoparticles yet allows low-molecular weight species, such as nanoparticle monomers and extra ligands, to permeate.

Recently, nano-sized materials have also seen use in biological imaging and the electronics industry due to their unique optical and electronic properties. The purification process for nanoparticles has been challenge to produce lower polydispersity and higher purity owing to the size-dependency up their electronic and optical properties. [7,8] Furthermore, extra side ligands or nanoparticle monomers have been shown to affect the stability and properties of nanoparticles. [9,10] Present separation methods, such as centrifugation [11], size-exclusion chromatography [11], and flow-field fractionation [12], have been limited by their time-intensive nature, large waste generation, and low production. Membrane filtration is an inherently "greener" process, requiring less solvent and time than other methods. The prediction of membrane performance is possible based on the stated pore size of the membrane, and scale-up for industrial purposes promises to be much easier than in conventional methods.

For 1-5 nm gold nanoparticles, a narrow size distribution was achieved from a post-synthetic mixture using commercial ultrafiltration membranes and a diafiltration technique. [13,14] However, these methods have been limited to application in situations where the average particle size was larger than 1 nm. In this work, the nanofiltration of subnanometer sized, tetrahydrofuran soluble, $Au_{11}(PPh_3)_8Cl_3$ (Au_{11}), with emphasis on interfacing to an upstream microreactor, is demonstrated. The ligand properties and small size of Au_{11} make it attractive as a catalyst for the oxidation of alcohols by H_2O_2, [15] and as a labeling agent for the stoichiometric conjugation with proteins [16]. Au_{11} has also been reported to be a precursor whose phosphine ligands can be replaced by thiolates or glutathione, which results in larger nanoparticles for other applications. [9,17]

In these studies, two different nanofiltration membranes were used; ceramic (Inopor® nano), and polymeric (DuraMem^{TM}500) materials. Ceramic membranes offer unique advantages relative to their organic polymer membrane counterparts. They are stable over a wide pH range (2-14), are resistant to most polar and non-polar solvents, and are stable, even at extremely high temperatures (~ 350˚C) [3,18,19]. The ceramic membranes were acceptable for aprotic solvent environments, such as tetrahydrofuran -soluble Au_{11}. Ceramic membrane media are expensive, and a thick support layer is needed to protect the fragile, active thin layer. Polymeric membranes have the limitation of modest operating temperature, but their advantages include their flexible shape and relatively low price. Solvent options are limited by the composition material of the polymeric membrane and swelling is a common problem. [1,3] Tetrahydrofuran,

however, is comparable with the DuraMem series membranes. [4] Both membranes showed the retention of Au_{11} “standard” and removal of byproducts such as PPh_3 and $AuClPPh_3$.

The continuous synthesis process, coupled with the nanofiltration system, resulted in a significant reduction in synthesis time while delivering a higher apparent yield than could be achieved in batch experiments. Filter cake formation was noted, and largely attributed to concentration polarization on the membrane surface, filtration speed, and electrostatic interaction between the filter and NPs. Tangential flow filtration, also called cross-flow filtration or diafiltration, is capable of reducing clogging, concentration polarization and other problems attributable to the dead-end flow geometry. The in-house built microextractor was designed to generate even cross-flow on commercial disk-filters [20], and achieved high-purity preparation of nanoparticles of low polydispersity.

2.3 Experiment

2.3.1 Chemicals

Hydrogen tetrachloroaurate ($HAuCl_4 \cdot 3H_2O$) was purchased from Strem Chemicals, Inc (Newburyport, MA, USA). Triphenylphosphine (PPh_3) and Sodium borohydride ($NaBH_4$) were purchased from Sigma Aldrich (St. Louis, MO, USA). The chemicals were used as received without further purification. All other reagents and solvents were purchased from Aldrich or VWR (Radnor, PA, USA) and were used as received.

Chloro(triphenylphosphine)gold(I) ($AuClPPh_3$ - precursor) was synthesized according to a previously described procedure [21], characterized by ^{1}H- and ^{31}P- NMR and UV-Vis data, and then used in the experiment as described.

2.3.2 Membranes

The ceramic membrane selected for use in this study was an Inopor® nano (inocermic GmbH, Hermsdorf, Germany) membrane with a molecular weight cut-off value of 450 Daltons. This membrane had a 47 mm diameter and an asymmetric structure, with a mean pore size of 0.9 nm. The active membrane layer was composed of TiO_2, which was deposited on a coarse-porous support (Al_2O_3 with 3 μm mean pore size) having a 2.5 mm combined thickness. DuraMem^{TM}500 (Membrane Extraction Technology, UK) was used as an organic-solvent resistant polymeric nanofiltration membrane. It was composed of a modified polyimide with a molecular weight cut-off [MWCO] of 500 Daltons.

2.3.3 Macroscale test fixture (MTF)

A macroscale test fixture, (Figure 2.1.a) constructed of opaque polyethylene terephthalate 0.5" thick (McMaster-Carr, Los Angeles, CA, USA), was machined using a shop lathe and mill and modified according to reference [22]. The fixture was designed for a 47 mm diameter ceramic membrane with an effective filtration area of 17 cm^2 and a channel height of 1.5 cm or a 35 mm diameter polymeric membrane with an effective filtration area of 10 cm^2 and a channel height of 0.25 cm. Both fixtures resulted in ~2.5 mL retentate volume. Gasketing was achieved with a PTFE-encapsulated silicon O-ring.

2.3.4 Microextractor

A microextractor was designed and fabricated for diafiltration (Figure 2.1.b). The microchannels were chemically etched to a depth of 250 μm on 3 mm thick stainless steel blank (McMaster-Carr) for the upper and lower substrates. Inlets and outlets were machined in place. The resulting geometry had 5.91 cm^2 of surface area available for filtration. A PTFE-encapsulated viton O-ring (McMaster-Carr) and a 2.5 mm stainless steel plate surrounded the membrane disc. A PTFE-encapsulated viton O-ring also sealed the upper and bottom microchannels plates. Three stainless steel membrane holders were sandwiched by thicker stainless steel plates with inlet and outlet holes as shown in Figure 2.1. The microextractor was designed for a counter-current flow in which pure solvent flow in the channels of the bottom plate swept away the permeate solution. To prevent the dilution of permeate solution by incoming solvent, this experiment was performed without a sweep of pure solvent.

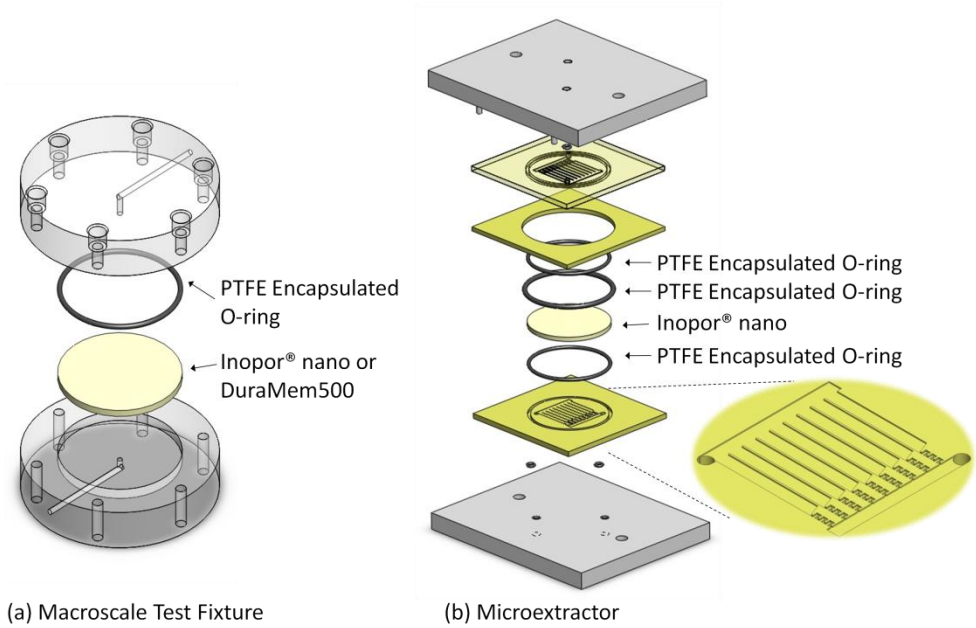

Figure 2.1 Diagram of the macroscale test fixture (MTF) [22] (a) and microextractor (b)

2.4 Experimental procedure

2.4.1 Material synthesis

Both the Au_{11} standard and post-synthetic Au_{11} solution were synthesized by reducing a tetrahydrofuran solution of $AuClPPh_3$ (40.5 mM) with $NaBH_4$ in ethanol (101.25 mM) in a home-built microreactor consisting of a T-mixer (P727, Upchurch Scientific, Oak Harbor, WA, USA) with connecting sections of 0.030" ID Teflon tubing (Upchurch Scientific). Each reactant solution was pumped into the reactor at 10 mL/min using a syringe pump (PHD 2000 Infusion/Withdraw pumps, Harvard Apparatus, MA, USA). The $AuClPPh_3$ solution was pumped into one arm of the tee, the $NaBH_4$ solution into another, and the third was the product outflow. The post-

synthetic Au_{11} solution was collected into a vial held at outlet. To generate an Au_{11} "standard" solution, quenching, solvent washing and recrystallization of the post-synthetic Au_{11} solution were performed. The chemistry was modified from a literature procedure presented previously. [9,10,23]

2.4.2 Fluidic controls

The membrane to be evaluated was mounted in the MTF and the microextractor was interfaced with dead-end (a) and cross (b) fluidic systems, respectively. (Figure 2.2) For dead-end flow filtration in the MTF, the feedstock was pressurized by supplying nitrogen (N_2) gas to the headspace. For cross flow filtration in the microextractor, a peristaltic pump (Upchurch Scientific) was used to drive the flow through the membrane and an N_2 gas head-pressure was applied to aid in the fine-tuning of the pressure drop across the membrane. The portions that passed through the membrane (permeate) and that were retained on the membrane (retentate) were collected for further characterization.

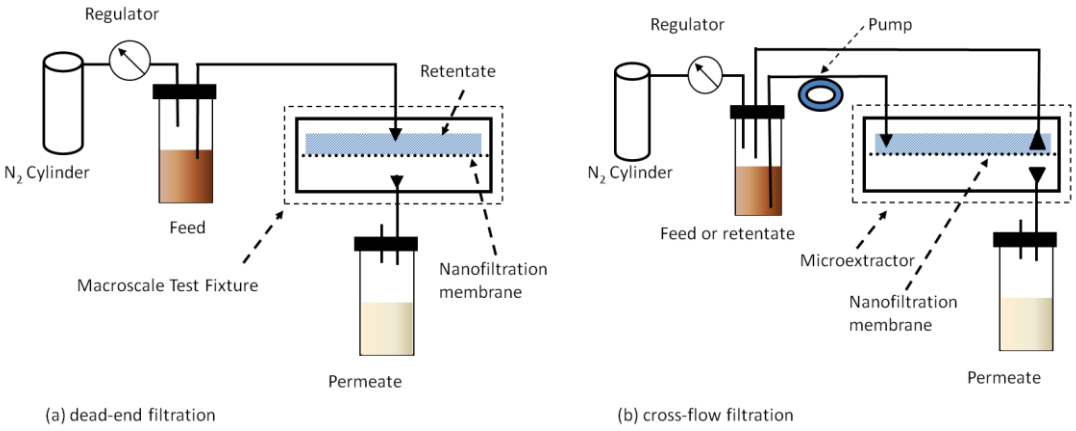

Figure 2.2 Fluidic schemes for dead-end flow filtration in the MTF (a) and for cross-flow filtration in the microextractor (b)

2.4.2.1 Dead-end flow filtration

Filtration experiments were conducted using various membranes in the MTF. N_2 at 1.4 bar was used as the driving force for filtration. The membranes were pre-conditioned with a mixture of 50% (v/v) tetrahydrofuran:ethanol (50% THF) until steady state fluxes were achieved. Thereafter, 5 mL or 10 mL of test solution (0.04 g/L Au_{11} standard, 10x diluted post-synthetic Au_{11}, 0.1 g/L PPh_3, or 0.1 g/L $AuClPPh_3$) was charged to a glass tube in a 250 mL Wheaton bottle, used with a PTFE adapter modified to accept ¼”-28 nuts and 1/16” O.D. PEEK tubing (Upchurch Scientific). In addition, an in-line experiment was conducted in which the output flow (total flow rate: 0.08 mL/min) of the microreactor was introduced directly to the MTF equipped with a membrane. (Figure 2.3)

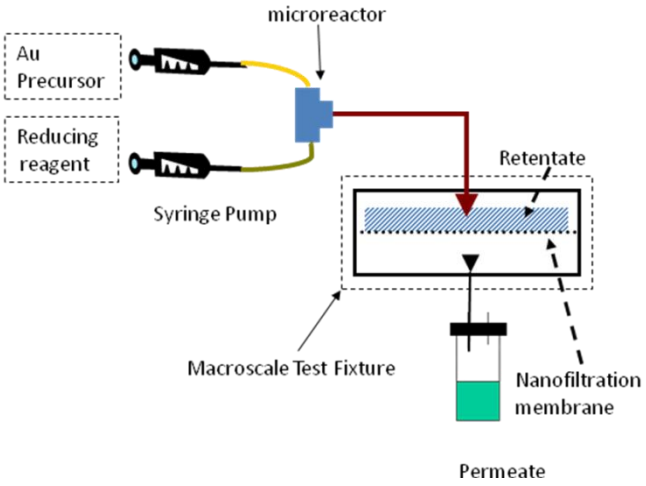

Figure 2.3 Fluidic control schematic for in-line microreactor and nanofiltration

2.4.2.2 Cross-flow filtration (Diafiltration)

The cross flow velocity through the channels was adjusted to 5 mL/min and the transmembrane pressure was fixed at 1.4 bar by adjusting the N_2 gas pressure in the solvent chamber. (Figure 2.2.b) Post-synthetic Au_{11} was diluted by 10x with 50% THF to facilitate filtration. An initial volume of 10 mL of 10x diluted post-synthetic Au_{11} with 50% THF was used for the first filtration. In subsequent steps, the retentate from the prior step was diluted with 50% THF to form a 10 mL of the feed volume.

2.4.3 Permeance and percent rejection measurement

Each membrane was pre-conditioned with pure solvent until a steady state flux was achieved. Solvent or solution volumetric fluxes were calculated based on mass flux and fluid density. Masses of each retentate and permeate were calculated by mass difference between the final and initial masses of vials collected over a fixed time interval.

Each feed, retentate, and permeate solution was diluted in a given amount of 50% THF and a UV-Vis spectrum was collected against a blank on an Agilent 8453 UV-Vis Spectrophotometer (Agilent, Santa Clara, CA, USA) from 190 nm to 800 nm using a quartz cuvette with a 1 cm path length. The observed rejection of the membrane was calculated as:

$$\text{Rejection}, R = \left(1 - \frac{C_{permeate}}{C_{retentate}}\right) \times 100$$

Where $C_{permeate}$ and $C_{retentate}$ are the final concentrations in the permeate and retentate, respectively.

For ^{31}P NMR spectroscopy, spectra were collected from samples dissolved in deuterated chloroform ($CDCl_3$), neutralized by basic alumina. For ^{31}P NMR spectroscopy (^{31}P, 161.98 MHz, Bruker 400 MHz NMR Spectrometer, Madison, WI, USA), the spectra were referenced to 85% H_3PO_4 (external standard).

2.5 Results and Discussion

Au_{11} rejection values were calculated by UV absorbance at 420 nm for the retentate and permeate solutions following the dead-end flow filtration of Au_{11} "standard" and post-synthetic Au_{11} using the MTF (Table 2.1). The "standard" and post-synthetic Au_{11} samples yielded rejection values of 93% and 65%, respectively, on the Inopor® nano membrane, and 82% and 88%, respectively, on the DuraMem^{TM}500 membrane. In addition, the anticipated low rejection values of PPh_3 and $AuClPPh_3$ (R

= 12% and 17%, respectively, on the Inopor® nano membrane and, R= ~0% and 4%, respectively, on the DuraMem™500 membrane) had molecular weights lower than each stated membrane's MWCO. Both membranes were shown to concentrate Au_{11} particles and remove PPh_3 and $AuClPPh_3$ from the post-synthetic Au_{11} solution.

Table 2.1 Rejection data for an Au_{11} standard and post-synthetic Au_{11}

	Macroscale test fixture (MTF) Rejection (%)				In-line filtration with a microreactor
	0.04 g/L Au_{11} Standard	10x diluted post-synthetic Au_{11}	0.1 g/L PPh_3	0.1 g/L $AuClPPh_3$	10x diluted post-synthetic Au_{11}
Inopor® nano[1)]	93 ± 3 %	65 %	12 ± 2 %	17 ± 2 %	67 %
DuraMem™500[2)]	82 ± 8 %	88 %[3)]	~0 %	4 ± 2 %	n/a

1) 5 mL of feed volume 2) 10 mL of feed volume 3) post-synthetic Au_{11} without dilution

The rejection of post-synthetic Au_{11} (R=65%) was shown to be lower than the Au_{11} standard solution (R=93%) on the Inopor® nano membrane using MTF (dead-end flow filtration). However, post-synthetic Au_{11} was filtered using the microextractor (cross-flow filtration) at 1.4 bar. A rejection of 97% was calculated from the UV-Vis data (Figure 2.4.a). The rejection values demonstrated an enhancement in rejection performance (with continuous flow) relative to the dead-end flow filtration approach.

In the dead-end flow filtration, the samples caked on the membrane, which caused membrane fouling (active filtration layer erosion and chemistry change) [3]. However, cross-flow swept away the buildup of material on the membrane surface and decreased the incidence of membrane fouling. Fouling membrane could be a factor in the decrease of membrane performance.

The UV-Vis and NMR data for diafiltration of post-synthetic Au_{11} in the microextractor provided for continuous removal of byproducts from the post-synthetic Au_{11} (Figure 2.4 and 2.5). The UV-Vis data of each diafiltration step provided 97% rejection of Au_{11}. The permeate UV-Vis spectrum showed the free ligand peak (PPh_3 at 255 ~ 280 nm) and the intensity of these peaks decreased with each subsequent step.

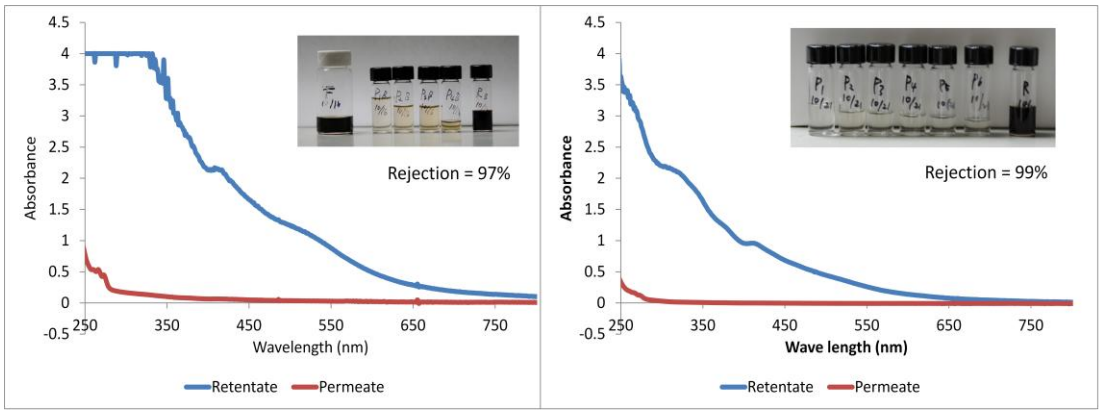

(a) Diafiltration step 1 of 10x diluted post-synthetic Au_{11} (b) Diafiltration step 2 of 10x diluted post-synthetic Au_{11}

Figure 2.4 UV-Vis spectrums of 10x diluted post-synthetic Au_{11} of each step in the microextractor using the Inopor® nano membrane. All samples were diluted by 10x to allow absorbance measurements. The photos of undiluted feed (F), permeate (P), and retentate (R) are inserted.

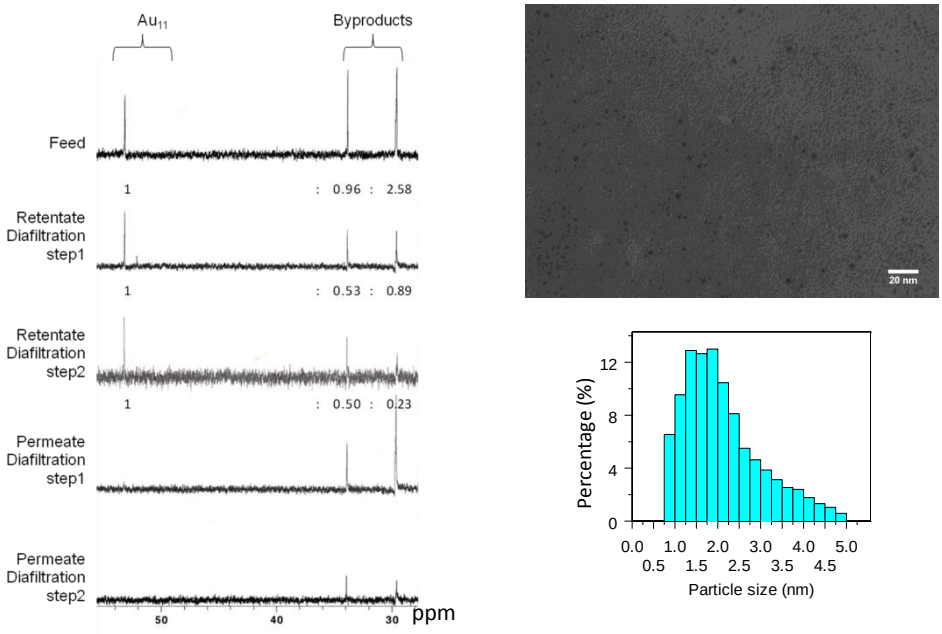

Figure 2.5 (a) ^{31}P NMR spectroscopy (^{31}P, 161.98 MHz) of diafiltration, retentate and permeate from the microextractor. The feed was diluted 10x in 50% THF. Step 1 retentate was used as the feed for the diafiltration step 2. The numbers below each peak represent the area ratio of each peak of Au_{11} and byproducts. (b) TEM image of retentate from step 2 and particle size distribution. The particle diameter was 1.4 ± 1.0 nm (n=2903)

In ^{31}P-NMR data of diafiltration of post-synthetic Au_{11} using the inopor® nano media, the permeate fraction showed only byproducts, and the retentate fraction contained the Au_{11} concentrated from the feed solution. (Figure 2.5) The extra ligand peak found at 29 ppm corresponded to a significant amount of free ligand in the feed solution. After the first filtration of the post-synthetic Au_{11} solution, the peak area ratio (0.89:1) of the ligand over the Au_{11} peak in retentate solution after the first step diafiltration decreased dramatically compared to the initial ratio (2.58:1) in feed solution. This retentate, diluted with 50% THF, was used as the feed of the second diafiltration step

and had the peak ratio 0.23:1 = free ligand: Au_{11}. The precursor ($AuClPPh_3$), unreacted or dissociated from the Au_{11}, was seen at 33 ppm. The relative amount of retentate in step 1 was also decreased by about 50%, but retentate in step 2 showed a similar ratio between Au_{11} and $AuClPPh_3$ because the purification time was extended in the second step; it is possible that some of the Au_{11} could have decomposed into $AuClPPh_3$. It was previously reported that byproducts of the Au_{11} reactions (and an impurity in many reaction mixtures of larger PPh_3-stabilized Au nanoparticles) led to the decomposition of Au_{11}. [10,24] The ^{31}P NMR spectrum showed the free ligand (29 ppm) and the precursor (33 ppm) of the permeate, and concentrated Au_{11} peak (53.2 ppm) of the retentate. A decreased ratio of the peak area of Au_{11} and byproducts was noted in each successive filtration step. Transmission electron microscopy (TEM) revealed a 1.4 ± 1.0 nm particle size. (Figure 2.5)

The rejection percentage of the in-line nanofiltration system was 67%. The high yield and high production rate of Au_{11} synthesis using a microreactor [23] suggests that it might be advantages to directly interface the nanofiltration system (for the post-synthetic Au_{11} purification) to upstream reactor, which would reduce the total production time.

A post-synthetic Au_{11} rejection value of 88% on the DuraMem^{TM}500 membrane showed that the polymeric membrane had a comparable rejection performance to the 83% rejection value of "standard" Au_{11}. The DuraMem^{TM}500 membrane was less affected by the post-synthetic Au_{11} filtration from the Inopor® nano membrane. [25]

Three consequent diafiltration experiments were also conducted with post-synthetic Au_{11} on the DuraMem^{TM}500 membrane using the MTF (dead-end flow filtration). The ^{31}P-NMR data confirmed the collection of Au_{11} in the retentate reservoir and the removal of PPh_3 and other byproducts in each permeate reservoir following diafiltration with the DuraMem^{TM}500 membrane (Figure 2.6).

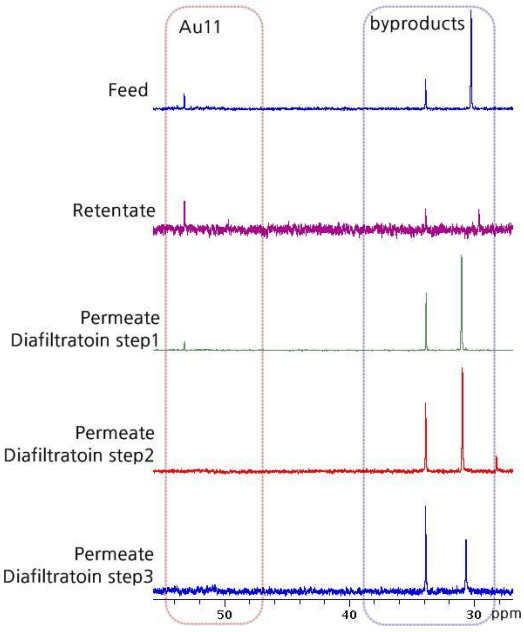

Figure 2.6 ^{31}P-NMR (^{31}P, 161.98 MHz) of feed, retentate, and permeate from diafiltration using DuraMem^{TM}500. The feed was post-synthetic Au_{11}. Permeate solution was collected and analyzed after each filtration, but the retentate solution was analyzed after the final filtration.

Table 2.2 Average flux (L m^{-2} h^{-1}) of 50:50 v/v THF:EtOH solvent in the MTF and the microextractor before and after post-synthetic Au_{11} filtration using the Inopor® nano membrane

	MTF (Dead-end flow)	Microextractor (Cross-flow)
J_w (L m^{-2} h^{-1})	8.74 ± 0.22	33.32 ± 1.32
J_a (L m^{-2} h^{-1})	2.26 ± 0.05	16.06 ± 0.63
J_a/J_w (%)	25.87 ± 0.83	48.21 ± 2.68

J_w – the pure solvent flux of the clean membrane
J_a- the permeate solvent flux after the filtration

The computational dynamic model of the microextractor improved the flow and pressure balance and made the distribution more uniform, which increased system performance as evidenced by an increase in throughput and simplified maintenance of the membrane. [20]

The MTF and microextractor were run at a 1.4 bar pressure drop, below the maximum differential pressure (1.5 bar) of the peristaltic pump. The solvent flux of the microextractor had a higher value than that for the MTF, thus the microextractor was capable of purifying higher amounts of solution per unit time. (Table 2.2) The ratio of J_a/J_w was correlated to the permeate flux loss due to the interaction between the post-synthetic Au_{11} and the membrane material, indicating membrane fouling. The J_a/J_w value measured for the microextractor was higher than those observed for the MTF,

which suggested that lower permeate flux loss occurred when using the microextractor than was the case for the MTF. This flux decrease for the ceramic nanofiltration membrane was reported also for the monolithic Inopor® nano ceramic membrane, which filtrated silage juice from a green biorefinery in water.[25]

2.6 Conclusion

In this article, we described how the nanofiltration membrane was capable of purifying the post-synthetic nanoparticles. The chemical resistances of ceramic and polymeric membranes were able to endure the non-aqueous solvent environments of nanoparticle synthesis; small pore sizes could retain the nanoparticles on the membrane, and byproducts, such as free-ligands and unreacted starting materials, passed through the membrane. Chemical and thermal robustness of the ceramic membranes enabled membrane reuse by cleaning the membrane in diluted acidic or basic conditions. The smallest nanoparticles filtration, using Inopor® nano and DuraMem^{TM}500 membranes, could be used to develop methods to purify or separate larger particles from the free ligands or unreacted reagents. In addition to less organic solvents being used in the nanoparticles synthesis, the nanofiltration made less organic waste and took less time than the formal, conventional purifications, demonstrating a greener purification method.

The microextractor was suitable to fit the membrane discs with different molecular weight cut-offs, so the various membranes with various pore sizes applied to filtrate different sizes of nanoparticle with the different solvent system. The microreactor coupled with the microextractor could be suitable for the continuous diafiltration system to achieve both membrane maintenance and increased treatment of nanoparticles synthesis.

2.7 References

[1] A.G.F. I, A. Schaefer, T.D. Waite, Nanofiltration: Principles and Applications, 1st ed., Elsevier Science, 2005.

[2] J.P. Sheth, Y. Qin, K.K. Sirkar, B.C. Baltzis, J. Membr. Sci. 211 (2003) 251-261.

[3] P. Vandezande, L.E.M. Gevers, I.F.J. Vankelecom, Chem. Soc. Rev. 37 (2008) 365-405.

[4] I. Sereewatthanawut, F.W. Lim, Y.S. Bhole, D. Ormerod, A. Horvath, A.T. Boam, A.G. Livingston, Org. Process Res. Dev. (2010).

[5] S. So, L.G. Peeva, E.W. Tate, R.J. Leatherbarrow, A.G. Livingston, Org. Process Res. Dev. 14 (2010) 1313-1325.

[6] C. Van Doorslaer, D. Glas, A. Peeters, A. Cano Odena, I. Vankelecom, K. Binnemans, P. Mertens, D. De Vos, Green Chem. 12 (2010) 1726.

[7] G.H. Woehrle, L.O. Brown, J.E. Hutchison, J. Am. Chem. Soc. 127 (2005) 2172-2183.

[8] G.H. Woehrle, M.G. Warner, J.E. Hutchison, Langmuir 20 (2004) 5982-5988.

[9] G.H. Woehrle, M.G. Warner, J.E. Hutchison, J. Phys. Chem. B 106 (2002) 9979-9981.

[10] L.C. McKenzie, Mechanistic Insights on Nanoparticle Formation: Investigation of Reaction Pathways and Development of Controlled Syntheses for Triphenylphosphine-stabilized Undecagold, PhD Dissertation, University of Oregon, 2009.

[11] J.P. Novak, C. Nickerson, S. Franzen, D.L. Feldheim, Anal. Chem. 73 (2001) 5758-5761.

[12] C. Contado, R. Argazzi, J. Chromatogr. A 1216 (2009) 9088-9098.

[13] A. Akthakul, A.I. Hochbaum, F. Stellacci, A.M. Mayes, Adv. Mater. 17 (2005) 532-535.

[14] S.F. Sweeney, G.H. Woehrle, J.E. Hutchison, J. Am. Chem. Soc. 128 (2006) 3190-3197.

[15] Y. Liu, H. Tsunoyama, T. Akita, T. Tsukuda, J. Phys. Chem. C 113 (2009) 13457-13461.

[16] S. Ariyasu, A. Onoda, R. Sakamoto, T. Yamamura, Dalton Trans. (2009) 3742.

[17] Y. Shichibu, Y. Negishi, T. Tsukuda, T. Teranishi, J. Am. Chem. Soc. 127 (2005) 13464-13465.

[18] A. Buekenhoudt, M. Reyes, M. dez Miguel, in:, Inorganic Membranes: Synthesis, Characterization and Applications, Elsevier, 2008, pp. 1-31.

[19] K. Li, Ceramic Membranes for Separation and Reaction, John Wiley and Sons, 2007.

[20] T. Kim, G.K. Lingam, B.K. Paul, V.T. Remcho, in:, MicroTas2009, The Chemical and Biological Microsystems Society, Jeju, South Korea, 2009, pp. 1210-1212.

[21] P. Braunstein, H. Lehner, D. Matt, Inorg. Synth. 27 (1990) 218-221.

[22] J.T. Rundel, B.K. Paul, V.T. Remcho, J. Chromatogr. A 1162 (2007) 167-174.

[23] Hyung Dae Jin, A. Garrison, T. Tseng, B.K. Paul, Chih-Hung Chang, Nanotechnology 21 (2010) 445604.

[24] G.H. Woehrle, J.E. Hutchison, Inorg. Chem. 44 (2005) 6149-6158.

[25] W. Koschuh, V.H. Thang, S. Krasteva, S. Novalin, K.D. Kulbe, J. Membr. Sci. 261 (2005) 121-128.

2.8 Acknowledgement

The authors gratefully acknowledge the financial support of the Air Force Research Laboratory via the Safer Nanomaterials and Nanomanufacturing Initiative (SNNI). We also thank Anna E. Garrison and Gopi K. Lingam for assistance with designing and fabricating the microextractror

Chapter 3 Separation of non-water-soluble nanoparticles by nanofiltration and ultrafiltration

3.1 Abstract

Nanofiltration and ultrafiltration are effective means of purifying nanoparticles, although they are labor-intensive processes and the membranes are expensive. We have developed in-line (post-reactor) nanofiltration tools that enhance membrane longevity and increase the speed of purification. Here, we demonstrate the application of organic-solvent-resistant nanofiltration and ultrafiltration membranes to the purification and size-based separation of lead sulfide nanoparticles and gold nanoparticles that were initially synthesized with a 2-6 nm size distribution. The nanofiltration membranes achieved rejection values greater than 95% for each of the nanoparticle samples and retained most of the nanoparticles in the desired size range. The membranes also exhibited high permeability, which resulted in reduced purification time. Ultrafiltration membranes were screened and successfully applied to the size fractionation of both lead sulfide nanoparticles and gold nanoparticles.

3.2 Introduction

Nanoparticles have received considerable attention because of their promise as semiconducting materials for photovoltaics, LEDs, and luminescence applications.

Lead chalcogenides such as PbS, PbSe, and PbTe exhibit unique properties because of their tunable first exciton wavelength at near-infrared (NIR) wavelengths, which can be tuned by controlling the size and bandgap of the nanoparticles. [1–3] This wavelength range makes lead chalcogenide nanoparticles applicable as optical amplifier media for telecommunications systems based on silica fiber technology. [2] Water-soluble PbS nanoparticles also have potential as fluorescence imaging agents because of the deep permeation depth of NIR wavelengths into and out of tissue though toxicity is of course a concern. [4] To meet these criteria, highly selective synthetic methods and/or post-synthetic separation methods are critical for the production of high-quality nanoparticles with narrow size distributions that produce narrow-bandwidth (full width at half-maximum, fwhm) absorption and emission. The fabrication of infrared devices such as photovoltaics, LEDs, and luminescent materials also demands high-quality nanoparticles with narrow size distributions that are soluble in organic solvents. [5] The hot-injection method produces high-quality, non-water-soluble nanoparticles. [1] Failure to control the growth temperature and period can affect the bandgap and broaden the size distribution of the resulting nanoparticles. [5,6] Post-synthetic processes such as solvent precipitation [7,8], centrifugation [9,10], size-exclusion chromatography [11,12], and membrane-based filtration [13–17] are often used to produce high-purity nanoparticles. Solvent precipitation and centrifugation methods require a significant amount of solvent and time to allow the configuration and development of the purification step. The sorbent in chromatography easily sorbs the desired nanoparticles, thus potentially decreasing product yield. The predictable

performance and long-term stability of membrane-based filtration methods could significantly reduce materials costs and energy consumption, while providing for increased yield and purity.

Membrane filtration has been utilized to separate and purify nanoparticles with some success, especially those that are water soluble. [13–16,18,19] Cross-flow ultrafiltration membranes have been used to separate water-soluble gold nanoparticles (AuNPs) and silver nanoparticles have been separated using the diafiltration method, respectively. [15,18] Microfiltration membranes have also been used to fractionate water-soluble polymer nanocapsules and polydisperse nanosized ferric oxide hydrates in the range of 10 to 100 nm by a dead-end flow filtration method. [13,16] The separation of non-water-soluble AuNPs by dead-end flow filtration was achieved using a PVDF-g-POEM graft copolymer ultrafiltration membrane. [14] Major limitations of the membrane, however, included the poor membrane stability in organic solvents and low permeate flow compared to other purification methods, such as centrifugation and size-selective precipitation. [19]

In this study, organic-solvent resistant ultrafiltration and nanofiltration membranes were used to purify and separate organic-soluble PbS nanoparticles as well as AuNPs. Two ultrafiltration membranes were evaluated: HFM-100 (Koch, Wilmington, MA, USA, molecular weight cut-off (MWCO) =50 kDa, PVDF) and MPF-U20S (Koch, MWCO=20kDa, composite). HFM-100 has been used as a water-soluble material for the separation of, for example, antibodies from egg yolk [20] and the pretreatment of

seawater. [21] The process of degumming crude soybean oil has been performed using MPF-U20S membrane filtration. [22] The commercially available membranes HFM-100 and MPF-U20S are compatible with organic solvents such methanol, ethanol, and toluene. Here, we have fractionated PbS nanoparticles and AuNPs (protected with oleic acid and dodecanethiol, respectively) using an ultrafiltration membrane in toluene. The PbS nanoparticles and AuNPs exhibited essentially the same initial size range, which allowed a direct comparison of the rejection performance. Nanofiltration membranes with pore sizes smaller than the PbS nanoparticles and AuNPs were utilized here to concentrate nanoparticles and remove extra side ligands and smaller nanoparticles from the post-synthetic products.

3.3 Experiment

3.3.1 Chemicals

Hydrogen tetrachloroaurate ($HAuCl_4 \cdot 3H_2O$) was purchased from Strem Chemicals (Newburyport, MA, USA). Triphenylphosphine (PPh_3) was purchased from Sigma-Aldrich (St. Louis, MO, USA). Borane-*tert*-butylamine complex and 1-dodecanethiol were purchased from Alfa Aesar (Ward Hill, MA, USA). The chemicals were used as received without further treatment. All other reagents and solvents were purchased from Aldrich or VWR (Radnor, PA, USA) and were used as received. Chloro(triphenylphosphine)gold(I) ($AuClPPh_3$- precursor) was synthesized according to a previously described procedure [23], characterized by ^{1}H NMR, ^{31}P NMR and UV–Vis spectroscopy, and then used in the described experiment.

3.3.2 Nanoparticles

A series of lead sulfide (PbS) nanoparticles capped with oleic acid were supplied by Voxtel (Beaverton, OR, USA). Each PbS "number" represents the λmax of the PbS nanoparticles. Gold nanoparticles capped with dodecanethiol were produced by the borane-*tert*-butylamine complex reduction of $AuClPPh_3$ and 1-dodecanethiol mixture according to the method of Stucky. [24] Briefly, 10 μL of dodecanethiol was added per 1 mL of a 40 mM $AuClPPh_3$ toluene solution, followed by the addition of an equal volume of 115 mM borane-*tert*-butylamine complex at room temperature, 55 ˚C and 100˚C for 2 nm, 6 nm, and 8 nm AuNPs, respectively. Particle sizes were determined by transmission electron microscopy (TEM), and UV–Vis–NIR spectra were obtained using a UV–Vis–NIR spectrophotometer.

3.3.3 Membranes

Membranes with the specifications presented in Table 3.1 were purchased from Membrane Extraction Technologies (London, UK), Sterlitech (Kent, WA, USA), and Spectrum Laboratories (Rancho Dominguez, CA, USA). Before use, each nanofiltration membrane was rinsed with fresh toluene at 5–20 psi to remove the preservation agents. Each ultrafiltration membrane was conditioned by sequentially washing it with water, methanol, and toluene. The membrane area was 10 cm^2 for all membrane types.

Table 3.1 Specifications of the membranes

Class[a]	Supplier	Membrane	MWCO[b] (Dalton)	Membrane Material	Chemical Compatibility	Maximum Pressure (bar)
NF	MET[c]	STARMEM™ 122	220	Polyimide (active form)	Alcohol, Alkanes, Aromatic	60
NF	MET[c]	DuraMem™ 900	900	Modified Polyimide (active form)	Polar aprotic, Alcohols, Aromatics, Ethers, Ketones	20
UF	Koch membrane	MPF-U20-S	20K	composite[f]		
UF	GE-Osmonics	JW	30K	PVDF[d]	-	-
UF	Koch membrane	HFM-100	50K	PVDF[d]	-	-

[a] UF: ultrafiltration; NF: nanofiltration

[b] Molecular weight cut-off, defined as MW, at which 90% rejection is obtained on the membrane

[c] Membrane extraction Technologies

[d] Polyvinylidene fluoride

[f] Composite is proprietary.

3.4 Experimental procedures

3.4.1 Filtration procedure

3.4.1.1 Dead-end flow filtration

The membrane experiments were performed in a custom-built dead-end flow membrane system. (Figure 3.1.a) The filtration device was constructed for nanofiltration and ultrafiltration membranes with a 35 mm diameter and a channel height of 0.25 cm. At the beginning of each experiment, fresh solvent was added to the feed vial, and each membrane was conditioned. After the fresh solvent had been removed, the feed vial was filled with a 5 mL or10 mL aliquot of nanoparticle solution and pressurized with 5 psi of N_2. A portion of the solution permeated through the membrane and collected in the vial (as permeate) by a certain time. The last portion of the permeate solution was used to calculate the rejection value. The concentrated portion (retentate, 2.5 mL) on the membrane was collected after filtration. A schematic flow diagram of the experimental setup is given in Figure 3.1.a. The permeate flux was calculated from measurements of the mass permeated per unit area of the membrane per unit time using the equation $J_p = M_p/(A \times t)$. The dead-end flow filtration experiments were conducted at room temperature. The concentration of nanoparticles in the feed, retentate and permeate fractions were determined after filtration. The rejection, *R*, of nanoparticles was used to assess the ability of the membrane to separate the nanoparticles between the permeate and retentate solutions. The rejection is defined by the equation $R= (1-C_P/C_R) \times 100\%$, where C_P and C_R are

the concentration of permeate and retentate solutions, respectively. A high rejection value indicates that more nanoparticles are retained by the membrane.

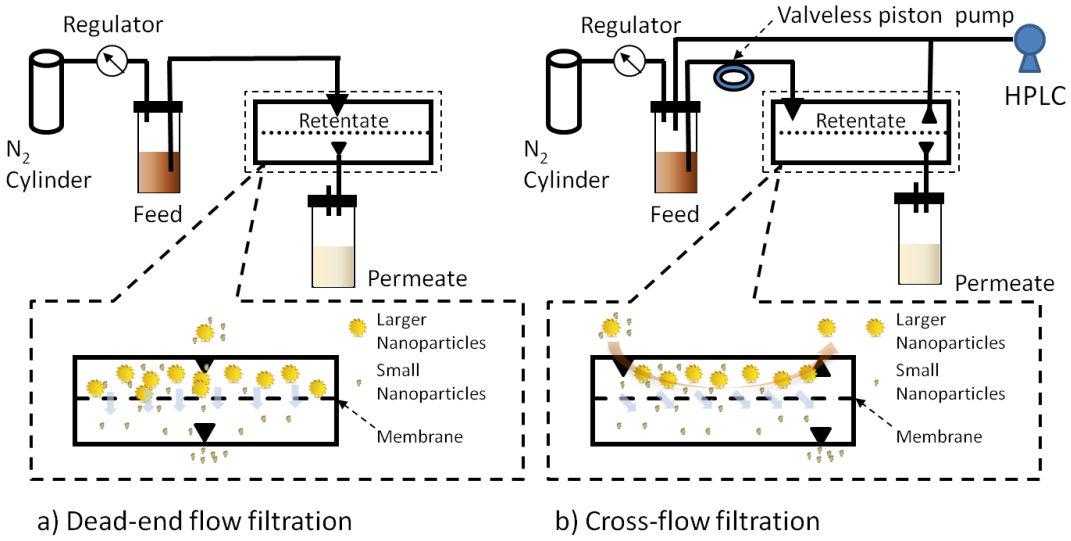

Figure 3.1 Schematic flow diagram for (a) dead-end flow filtration and (b) cross-flow filtration

3.4.1.2 Cross-flow filtration

A cross-flow filtration system was applied to the separation of PbS nanoparticle mixtures PbS880 (~2.1 nm) and PbS1400 (~4.9 nm) using an HFM-100 membrane. The feed solution was drawn from the reservoir the membrane through a valveless piston pump (cross-flow rate: 2 mL/min, ISMATEC, IDEX-HS, WA, USA). Nitrogen gas was used to maintain a 5 psi pressure drop across the membrane. An external HPLC pump provided fresh solvent to maintain the feed solution volume for

diafiltration. (Figure 3.1.b) The retentate solution was collected when the total permeate solution exhibited twice the weight of the initial feed solution.

3.4.2 Characterization of nanoparticles

The UV–Vis–NIR spectrum of each feed, retentate, and permeate solution was measured using one of two UV–Vis–NIR spectrophotometers: A JASCO V-670 (Easton, MD, USA) or an Agilent 8453 (Santa Clara, CA, USA). The samples were dispersed in 1 cm path length quartz cells filled with toluene. The absorbance values at each nanoparticle solution's λmax of the first exciton were used to calculate the rejection values. The particle sizes and distributions were determined using a Philips CM-12 scanning transmission electron microscope operated at an acceleration voltage of 120 kV. TEM samples were prepared from a dilute solution of particles in toluene that was dropcast on a 300-mesh copper TEM grid that contained a Formvar–carbon support film (Electron Microscopy Science, PA, USA); the samples were dried by N_2 gas and air. Transmission electron microscopy (TEM) images were analyzed using the image-processing software NIH Image J. [25]

3.5 Results and Discussion

3.5.1 Nanoparticles

We characterized the UV–Vis–NIR spectra and the particle-size distributions of a series of PbS nanoparticles. (Figure 3.2-a) A given size series of PbS nanoparticles was characterized as a function of the λmax of the first exciton and of the particle size as measured by TEM. Figure 2 shows the series of PbS nanoparticles as a function of their λmax of the first exciton. As the particles become larger, the λmax increases. [1,26] The correlation of the size (as measured by TEM) as a function of the λmax of the PbS nanoparticles are represented in the inset graph of Figure 3.2. Figure 3.2.b represents the absorbance spectra of organic-soluble gold nanoparticles with various sizes that were synthesized by the method of Stucky [24]; the samples exhibit surface plasmon resonance (SPR) at 520 nm.

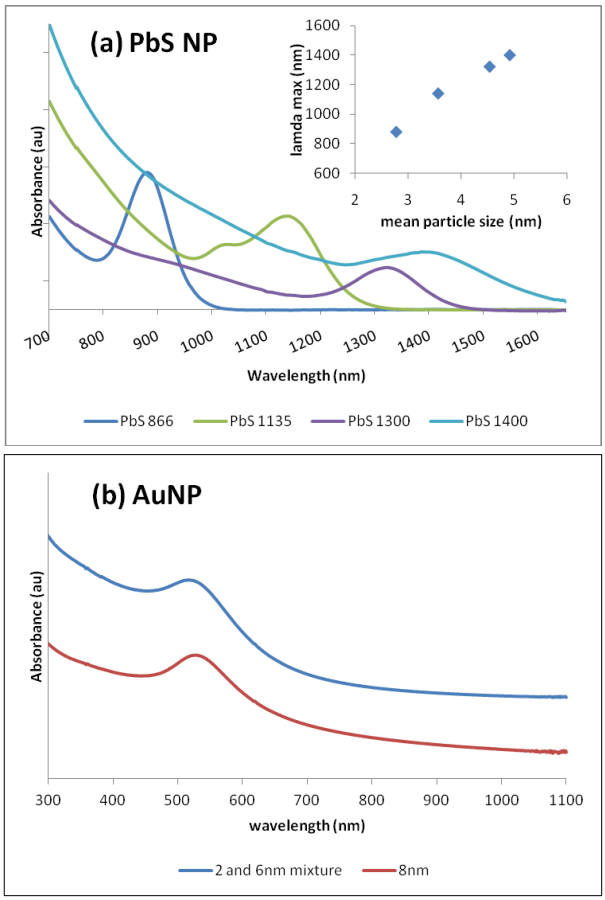

Figure 3.2 The λmax of the first exciton of a size series of PbS nanoparticles (a). The inset graph contains a plot of the size of the PbS nanoparticles as a function of the λmax. Smaller nanoparticles require a shorter wavelength (higher energy) of excitation. Each PbS "number" represents the λmax of the PbS nanoparticles. The spectra of AuNPs (b) show the surface plasmon resonance.

3.5.2 Nanoparticles filtrations

3.5.2.1 Lead sulfide nanoparticle (PbS NP) filtration

The performance of each membrane was assessed using PbS nanoparticles in toluene. The absorbances at each λmax of the first exciton of the PbS nanoparticles and the SPRs of the AuNPs were employed for the determination of the rejection performance of the nanoparticles when nanofiltration and ultrafiltration membranes were used. Table 3.2 shows the rejection values and permeabilities that correspond to each class of the PbS nanoparticles and AuNPs.

The STARMEM^{TM}122 and DuraMem^{TM}900 nanofiltration membranes exhibited rejection values greater than 95% for the PbS nanoparticles, which indicates that most of the PbS nanoparticles were retained on the membranes. The higher rejection values for PbS nanoparticles on these nanofiltration membranes suggest that they maybe useful for the removal of unreacted free ligands from the post-synthetic PbS nanoparticles. The results in Table 2b indicate that the average for the STARMEM^{TM}122 and DuraMem^{TM}900 permeabilities for the PbS nanoparticles were ~4 and ~42 kg m^{-2} hr^{-1} bar^{-1}, respectively. DuraMem^{TM}900 clearly exhibits a greater experimental permeability and is better suited to mass-production purification operations than is STARMEM^{TM}122. The low permeability of STARMEM^{TM}122 indicates a lower affinity of the semi-hydrophilic membrane toward apolar solvents such as toluene and *n*-hexane. [27]

Table 3.2 Rejection and permeability (kg m^{-2} hr^{-1} bar^{-1}) of each PbS and AuNP nanoparticle solution using commercially available nanofiltration and ultrafiltration membranes in toluene.

(a) Rejection

Median particle size (nm)	PbS866 2.8	PbS1135 3.6	PbS1300 4.5	PbS1400 5.0	AuNP 2 and 6	AuNP 8
STARMEM™122	95.3%	98.0%	95.0%	99.0%	-	-
DuraMem™900	95.6%	97.5%	99.4%	98.6%	95.5%	95.3%
JW	-	-	-	17%	-	-
HFM-100	0%	-	-	65.9%	96%	96.3%
MPF-U20S	0%	0%	-	10.4%	21.7%	94.5%

(b) permeability (kg m^{-2} hr^{-1} bar^{-1})

Median particle size (nm)	PbS866 2.8	PbS1135 3.6	PbS1300 4.5	PbS1400 5.0	AuNP 2 and 6	AuNP 8
STARMEM™122 60psi 10mL sample solution	4	5	4	4	-	-
DuraMem™900 5psi 10mL sample solution	40	48	44	37	101	79
JW 5psi 10mL sample solution	-	-	-	195	-	-
HFM-100 5psi 10mL sample solution	229	-	-	144	270	245
MPF-U20S 5psi 5mL sample solution	311	-	-	381	292	354

Filtration performed at 23-25˚C. Each 10 mL feed solution (0.1 g/L) was subjected to filtration separately at a certain pressure (STARMEM™122 = 60psi, DuraMem™900, JW, HFM-100, and MPF-U20S = 5psi)

Compared to the higher rejection values achieved for PbS nanoparticles during organic-solvent nanofiltration, the ultrafiltration membrane exhibits selective rejection values that depend on the particle size. The 5.0 nm PbS nanoparticles, PbS1400, resulted in a lower rejection value (17%, higher permeation) on the JW and MPF-U20S membranes, and a moderate rejection value (65.9%) on the HFM-100 membrane. The 2.8 nm PbS nanoparticles, PbS866, were not retained on the HFM-100 membrane. MPF-U20S showed no retention of 2-5 nm PbS nanoparticles. (Table 3.2) These selective rejections indicate that HFM-100 will separate PbS nanoparticles with sizes below a certain threshold. A mixture of 0.5 mg/mL PbS880 and 0.5 mg/mL PbS1400 was treated by dead-end filtration using an HFM-100 membrane, which yielded rejection values of 0% and 65.9% for PbS880 and PbS1400, respectively. The solutes were removed from the retentate solution by volume reduction, followed by re-dilution with toluene and re-ultrafiltration in repeated steps (diafiltration). After three sequential diafiltration steps, the retentate and permeate solutions were collected and analyzed using UV–Vis–NIR and TEM. The spectrum of the retentate solution confirms the removal of the PbS880 and the retention of the PbS1400. (Figure 3.3) However, the spectrum of the permeate solution confirms the presence of both PbS880 and PbS1400. (Figure 3.3.d)

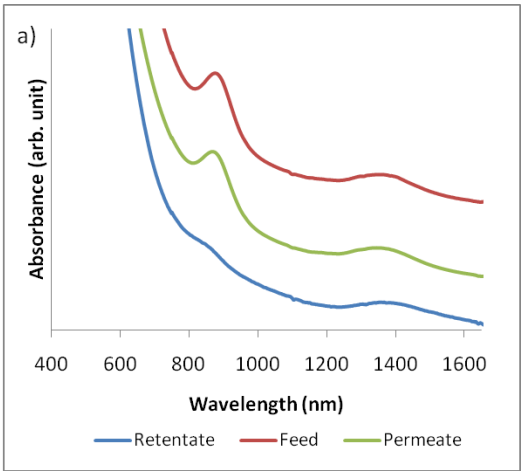

(b) Feed 2.6 ± 1.4 nm

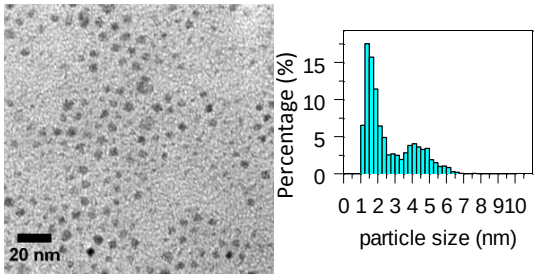

(c) Retentate 3.8 ± 1.3 nm

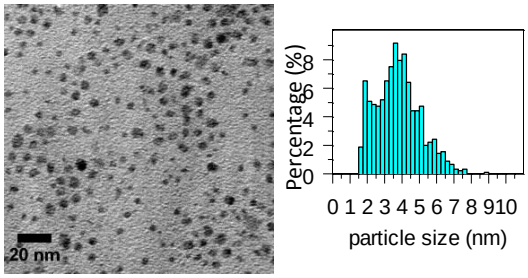

(d) Permeate 2.3 ± 1.2 nm

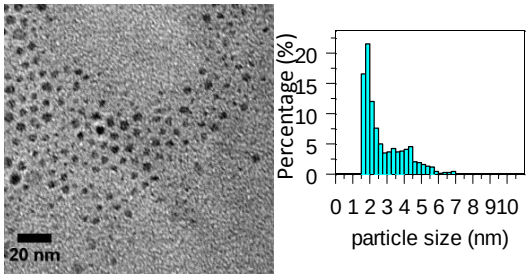

Figure 3.3 (a) UV–Vis–NIR absorbance spectra and TEM images of the (b) feed, (c) retentate, and (d) permeate of a mixture of PbS nanoparticles. A particle-size histogram is overlaid on each TEM image.

A cross-flow filtration system was also applied to the purification of PbS nanoparticle mixtures PbS880 and PbS1400 using an HFM-100 membrane. Reductions in the flow rate and the retention of particles, which are attributed to filter "caking," are endemic to the dead-end flow filtration method. A cross-flow perpendicular to the filtration direction proved effective in reducing the clogging of the membrane pores, and this is a scalable method that allows continuous-flow operation. The removal of the PbS880 and the retention of the PbS1400 are confirmed by the UV–Vis–NIR spectra of the retentate solution (R). (Figure 3.4) The spectra of the permeate solutions (Figure 3.4.a, P1-P5) show a sequential decrease of PbS880 but also indicate the presence of PbS1400. The histogram of the feed solution (4B) exhibits the expected bimodal distribution and suggests a mean particle size of 3.7 ± 1.6 nm. The particle-size distribution of the retentate solution (4C) indicates that the PbS1400 nanoparticles have a mean particle size of 4.7 ± 0.9 nm after filtration (and, more importantly, are highly enriched). These results indicate that the cross-flow filtration method using the HFM-100 membrane is capable of effectively purifying and concentrating PbS nanoparticles in the desired size range.

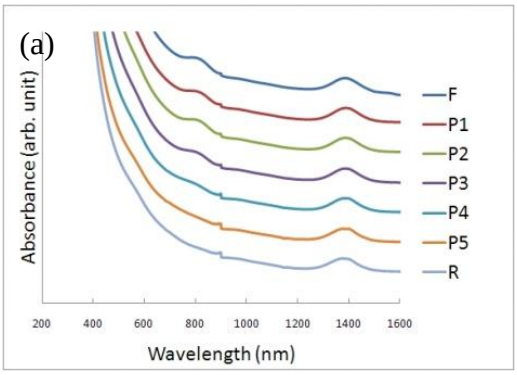

(b) Feed (F) 3.7 ± 1.6 nm

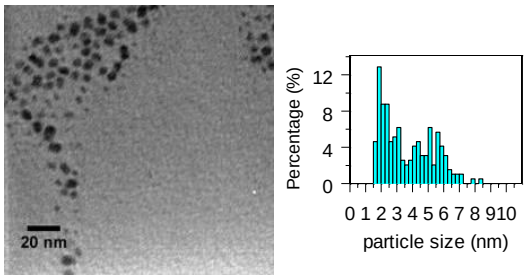

(c) Retentate (R) 4.7 ± 0.9 nm

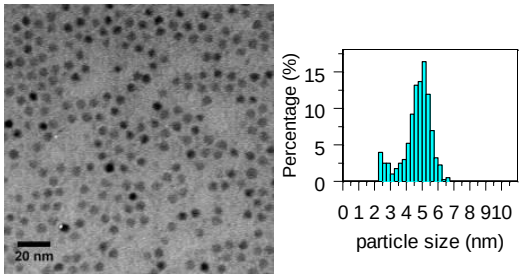

Figure 3.4 (a) UV–Vis–NIR absorbance spectra of the feed (F), permeate (P), and retentate (R) of PbS880 and PbS1400 mixtures. Each spectrum is normalized at 1389 nm. TEM images and histograms for (b) feed solution of the initial mixture of PbS880 and PbS1400 and for (c) the retentate solution after filtration.

3.5.2.2 Gold nanoparticle (AuNP) filtration

Two different size ranges of thiol-protected gold nanoparticles (2-6 nm AuNP and 8 nm AuNP) were separately filtered through each ultrafiltration and nanofiltration membrane. UV–Vis analysis of the retentate and permeate were conducted to quantify purification efficiency using rejection (%) as a metric. Each feed and permeate solution was studied by monitoring the changes in the particle-size distribution using TEM. The 2-6 nm AuNPs demonstrated retention on DuraMem^{TM}900 and HFM-100 (R=95.5% and 96%, respectively) but pervasion on MPF-U20S (R=21.7%); no retention was observed for this range of particle sizes. (Table 2) After the 2-6 nm AuNPs were filtered through the MPF-U20S membrane, a permeate particle size of 2.4 ± 0.6 nm was measured using TEM. This particle-size distribution represents an impressive improvement (narrowing) in the particle-size distribution. The percent relative standard deviation [%RSD] was 25.0% in the permeate, whereas the %RSD in the particle-size distribution for the feed was 48.8%. (Figure 3.5) The 8 nm AuNPs demonstrated retention on HFM-100 (R=96.3%), DuraMem^{TM}900 (R=95.3), and MPF-U20S (R=94.5%). (Table 3.2) No particles from the permeates of either HFM-100 or MPF-U20S could be detected using TEM. The absorbance spectra of the retentates of both membranes show a decrease relative to the absorbance of the feed solution of 6 nm AuNPs; this difference may be caused by nanoparticles becoming trapped in and fouling the membrane.

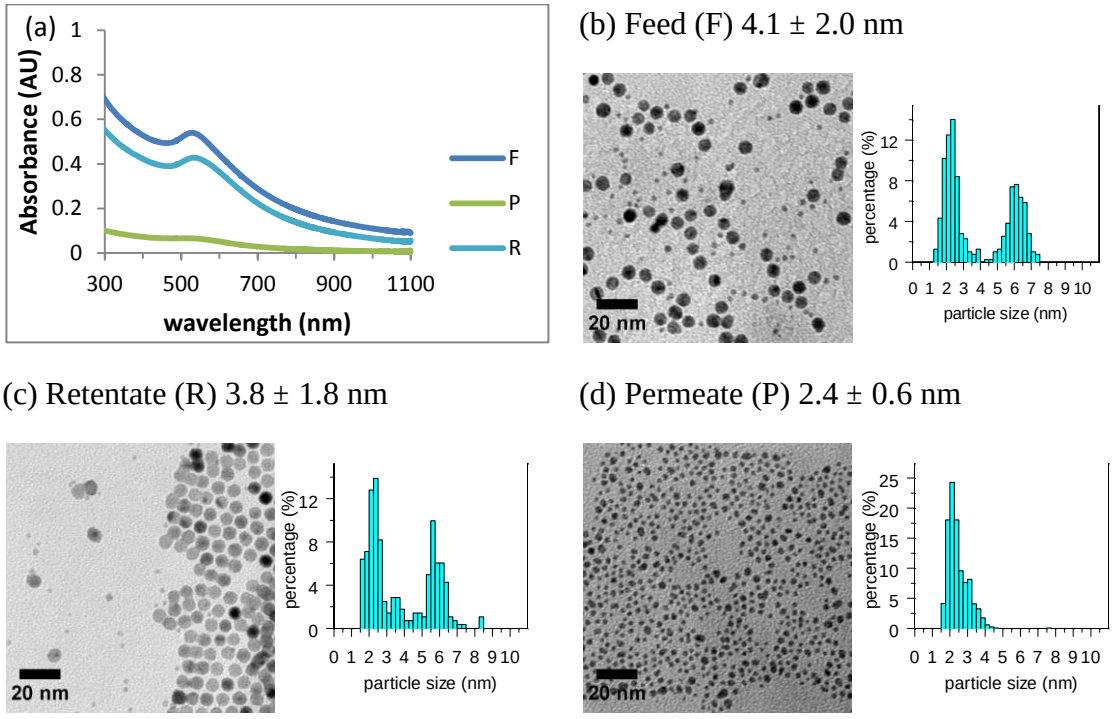

Figure 3.5 (a) UV–Vis–NIR spectra, TEM images and histograms for (b) the feed solution of initial 2-6 nm AuNPs, (c) the retentate and (d) permeate solution after filtration using MPF-U20S.

We separated different sizes of PbS nanoparticles and AuNPs using HFM-100 and MPF-U20S, respectively. Based on the rejection performance of these two membranes, we estimated that the HFM-100 membrane with a MWCO of 50 kDa can separate nanoparticles larger than 5 nm, and that a MPF-U20S membrane with a MWCO of 20 kDa can retain nanoparticles larger than 3 nm. However, experimental results have shown that HFM-100 fractionates 2-5 nm PbS nanoparticles and retains 2-8 nm AuNPs, while MPF-U20S permeates 2-5 nm PbS nanoparticles and fractionates 2-8 nm AuNPs. (Table 2) The stated MWCO of each membrane has limitations in an organic-solvent system, because the MWCO was characterized in aqueous media and is therefore not valid for estimations of the rejection performance of organic-soluble nanomaterials in organic solvent systems. The initial polymeric membrane structure is unlikely to be sustained in an exposure to an organic solvent. Swelling leads to pore size changes in membranes, and changes were seen in the rejection performance of MFP-U20S. [28] Even if each PbS nanoparticle and AuNP sample exhibits a comparable size range, the chemical properties of the protecting layer for each type of nanoparticle is likely to exhibit a different affinity for each membrane; therefore, each membrane will produce results that differ from the estimated rejection value based on the membrane's stated MWCO. Standardization is clearly a necessity.

3.6 Conclusion

Commercially available organic-solvent-resistant nanofiltration and ultrafiltration membranes were applied to the purification and separation of nanoparticles of various sizes. The nanofiltration membrane exhibited a molecular-weight cut-off less than the size of PbS nanoparticles and AuNPs, which resulted in high rejection values (R > 95%) and retention of the nanoparticles on the membranes. These membranes were utilized to concentrate nanoparticles and to remove undesired smaller nanoparticles and byproducts from post-synthetic nanoparticle mixtures. The HFM-100 and MPS-U20S membranes exhibited different rejection values based on the size of the PbS nanoparticles and AuNPs. These results indicate that both membranes are capable of effectively purifying and concentrating nanoparticles in the desired size ranges. However, the HFM-100 and MPS-U20S membranes exhibit different rejection values of similarly sized PbS nanoparticles and AuNPs. This difference may result from the interaction between the protecting layer of the nanoparticles and the membrane or between the solvent and the membrane.

3.7 References

[1] M.A. Hines, G.D. Scholes, Adv. Mater. 15 (2003) 1844-1849.

[2] A.L. Rogach, A. Eychmüller, S.G. Hickey, S.V. Kershaw, Small 3 (2007) 536-557.

[3] I. Moreels, K. Lambert, D. Smeets, D. De Muynck, T. Nollet, J.C. Martins, F. Vanhaecke, A. Vantomme, C. Delerue, G. Allan, Z. Hens, ACS Nano 3 (2009) 3023-3030.

[4] X. Gao, Y. Cui, R.M. Levenson, L.W.K. Chung, S. Nie, Nat. Biotech. 22 (2004) 969-976.

[5] H. Li, D. Chen, L. Li, F. Tang, L. Zhang, J. Ren, CrystEngComm 12 (2010) 1127.

[6] T.-Y. Liu, M. Li, J. Ouyang, M.B. Zaman, R. Wang, X. Wu, C.-S. Yeh, Q. Lin, B. Yang, K. Yu, J. Phys. Chem. C 113 (2009) 2301-2308.

[7] C.B. Murray, D.J. Norris, M.G. Bawendi, J. Am. Chem. Soc. 115 (1993) 8706-8715.

[8] A. Chemseddine, H. Weller, Ber. Bunsen-Ges. Phys. Chem. 97 (1993) 636-7.

[9] X. Sun, S.M. Tabakman, W. Seo, L. Zhang, G. Zhang, S. Sherlock, L. Bai, H. Dai, Angew. Chem. Int. Ed. 48 (2009) 939-942.

[10] L. Bai, X. Ma, J. Liu, X. Sun, D. Zhao, D.G. Evans, J. Am. Chem. Soc. 132 (2010) 2333-2337.

[11] T. Siebrands, M. Giersig, P. Mulvaney, C.H. Fischer, Langmuir 9 (1993) 2297-2300.

[12] S. Knoppe, J. Boudon, I. Dolamic, A. Dass, T. Bürgi, Anal. Chem. 0 (2011).

[13] I. Limayem, C. Charcosset, H. Fessi, Sep. Purif. Technol. 38 (2004) 1-9.

[14] A. Akthakul, A.I. Hochbaum, F. Stellacci, A.M. Mayes, Adv. Mater. 17 (2005) 532-535.

[15] S.F. Sweeney, G.H. Woehrle, J.E. Hutchison, J. Am. Chem. Soc. 128 (2006) 3190-3197.

[16] Q.-L. Xie, J. Liu, X.-X. Xu, G.-B. Han, H.-P. Xia, X.-M. He, Sep. Purif. Technol. 66 (2009) 148-152.

[17] D. Jassby, S.-R. Chae, Z. Hendren, M. Wiesner, J. Colloid Interface Sci. 346 (2010) 296-302.

[18] J.C. Trefry, J.L. Monahan, K.M. Weaver, A.J. Meyerhoefer, M.M. Markopolous, Z.S. Arnold, D.P. Wooley, I.E. Pavel, J. Am. Chem. Soc. 132 (2010) 10970-10972.

[19] B. Vanderbruggen, M. Manttari, M. Nystrom, Sep. Purif. Technol. 63 (2008) 251-263.

[20] H. Kim, S. Nakai, J. Food Sci. 63 (1998) 485-490.

[21] H.K. Shon, S.H. Kim, S. Vigneswaran, R. Ben Aim, S. Lee, J. Cho, Desalination 238 (2009) 10-21.

[22] C. Pagliero, N. Ochoa, J. Marchese, M. Mattea, J. Am. Oil Chem. Soc. 78 (2001) 793-796.

[23] P. Braunstein, H. Lehner, D. Matt, Inorg. Synth. 27 (1990) 218-221.

[24] N. Zheng, J. Fan, G.D. Stucky, J. Am. Chem. Soc. 128 (2006) 6550-6551.

[25] Image J 1.42. This Is a Shareware Image Processing Program. Rsbweb.nib.gov/ij/download.html, n.d.

[26] G.D. Scholes, Adv. Funct. Mater. 18 (2008) 1157-1172.

[27] S. Darvishmanesh, J. Degrève, B. Van der Bruggen, Phys. Chem. Chem. Phys. 12 (2010) 13333.

[28] R. Shukla, M. Cheryan, J. Membr. Sci. 198 (2002) 75-85.

Chapter 4 Separation and Purification of Nanoparticles using a Novel Templated Silsesquioxane Membrane

4.1 Abstract

A templated silsesquioxane (ssq) membrane was synthesized on a porous alumina support and used for the separation and purification of nano-sized materials, such as nanoparticles and macromolecules. The ssq membrane was fabricated by polycondensation of a silsesquioxane monomer solution in the presence of a surfactant within the macroporous space of an alumina membrane. The ssq membrane was annealed at 120˚C and subsequently washed with ethanol to remove the surfactant template from the membrane matrix. The ssq membrane was evaluated using 5-8 nm gold nanoparticles (protected with dodecanethiol) in chloroform. Following filtration, it was determined by transmission electron microscopy that the average particle size of the permeate was 4.4 ±0.6 nm, indicating the separation efficacy of the membrane. Myoglobin (~3.2 nm; 17 kDa) and bovine serum albumin (~7.2 nm, 66 kDa), prepared in 2-(N-morpholino)ethanesulfonic acid buffer solution, were also used to determine the membrane performance. Rejection values of 31.8% and 97.a% were determined for these test probes by UV-Vis assays of the permeate and the retentate, respectively. These results indicate that the ssq membrane has the desired size cut-off of 5 nm.

4.2 Introduction

Methods for the fabrication of nanochannels and pores have received much attention due to their great their potential in optical and chemical applications. One approach to their synthesis is to use macroporous filtration media as scaffolds for growth of mesoporous media, in essence the template consolidates the nanoporous component in the pore cavities. [1] Membrane filters with nano-sized pores have been developed for the food and biological industries to separate macromolecules, such as proteins and viruses,[2] and has recently been extended to the purification and separation of nanomaterials. Because an estimation of membrane performance can be made from pore size, in-situ separation using membrane filters coupled with a downstream reactor have been used for simple scale-ups into industrial manufacturing.

For templating purposes, the pore should be of non-tortuous geometry and range from 2 – 100 nm for the creation of nano-sized pores for ultrafiltration and microfiltration membranes. However, material selection and preparation methods place limits on the shape and size of the pore. Polycarbonate or polyester track-etched membranes have 1D pores suitable for use as a template for 2D nano-sized materials, but these polymers have thermal and chemical limitations. [3–5] Porous anodisc alumina membranes (AAM, Whatman, CO. Ltd., Maidstone UK) also have 1D pores and show strong thermal resistance and broad solvent compatibility; they are not subject to show polymeric deformation but are fragile due to their thin ceramic layer (60 μm). Because of its useful properties as a template, AAM is widely used to fabricate 2D nanomaterials, such as nanotubes, nanorods, and nanowires. [6–8]

Commercially available nanofiltration and ultrafiltration membranes have been limited by their tortuous pore geometry. To estimate the pore size via a sieving experiment, the rejection of size-defined materials, such as branched and linear alkanes of increasing molecular weight, are often measured. [9–13] Even commercially available non-tortuous pore membranes have a minimum pore size of 20 nm when alumina, polycarbonate, or polyesters are used as the substrate. Periodic mesoporous materials are attractive because of their high surface area, uniform pore size, and ordered pore arrangement. The organically modified silica, silsesquioxane (ssq), is an organic-inorganic hybrid material that offers both the design flexibility of various functional groups and a rigid framework. [14,15] Its self-assembly properties under acidic or basic conditions on a surfactant scaffold provide a periodic mesoporous structure. However, the mesoporous hexagonal channels of ssq prefer to be aligned parallel to the substrate's surface when fabricated as thin-layer forms. The transportation of molecules across this type of ssq film is not facile. To address this issue, our group and others have used the pores of AAM as a scaffold for growth of ssq nanochannels. [7,8] The uniform cylindrical pores are regularly oriented and exposed at the surface; thus, precursor (ssq) and surfactant (structure-directing agent) solutions are filled into the pores via aspiration. [16] The solvent is then evaporated, allowing for the construction of the mesostructured organic-inorganic material on the surfactant micelle scaffold. Finally, the surfactants are removed by calcination or a solvent extraction process. The methods for growing mesoporous silica within an AAM and the applications of this method have been reviewed. [7,8]

In the work described here, a templated silsesquioxane (ssq) membrane was synthesized on an AAM and used for the separation and purification of nano-sized materials such as nanoparticles and macromolecules. The ssq membrane was fabricated by polycondensation of a silsesquioxane monomer solution in the presence of surfactants within the macroporous space of an AAM. The ssq membrane was evaluated using organic-soluble, 5-8 nm gold nanoparticles and macromolecules such as myoglobin and bovine serum albumin.

4.3 Experimental

4.3.1 Chemicals and procedure

4.3.1.1 Chemicals

Hydrogen tetrachloroaurate ($HAuCl_4 \cdot 3H_2O$) was purchased from Strem Chemicals (Newburyport, MA, USA). Cetyltrimethylammonium bromide (CTAB), cetyltrimethylammonium chloride, triphenylphosphine (PPh_3), MES monohydrate, and 1,2-bis(triethoxysilyl)ethane (BTSE) were from Sigma-Aldrich Company Ltd. (St. Louis, MO, USA). The proteins myoglobin (from horse skeletal muscle, M-0630) and bovine serum albumin (BSA, Fraction V, A9647) were purchased from Sigma-Aldrich Company Ltd. (St. Louis, MO, USA). Ethanol and chloroform were from Aaper Alcohol (Shelbyville, KY, USA). Water was purified with a Millipore (Billerica, MA, USA) system (18.2 MΩ). Anodisc® alumina membranes with a pore size of 100 nm, a diameter of 47 mm, and a thickness of 60 μm were purchased from Whatman, CO.

Ltd. Chloro(triphenylphospine)gold(I) ($AuClPPh_3$) was synthesized by the reaction of hydrogen tetrachloroaurate ($HAuCl_4 \cdot 3H_2O$) with triphenylphosphine (PPh_3) as described in the literature. [17]

4.3.1.2 Silsequioxane membrane fabrication

The ssq membrane was fabricated by polycondensation of a silsesquioxane monomer solution in the presence of a cationic surfactant within the macroporous space of the AAM. [18] A solution containing a mixture of bis(triethoxysilyl)ethane (BTSE), HCl, H_2O, EtOH, and cetyltrimethylammonium bromide (CTAB) as the surfactant, in a molar composition of 1: 0.02:79.90:32.97:0.16, respectively, was added dropwise to the AAM. With gentle-to-moderate aspiration (vacuum was applied to the back side of the membrane during the application of the solution), the solution filled the pore spaces of the AAM, and the formation of ordered ssq channels was achieved by solvent evaporation-induced self-assembly. (Figure 4.1) To remove the surfactant template from the ssq channels, the ssq membrane was annealed at 120˚C and subsequently washed with ethanol.

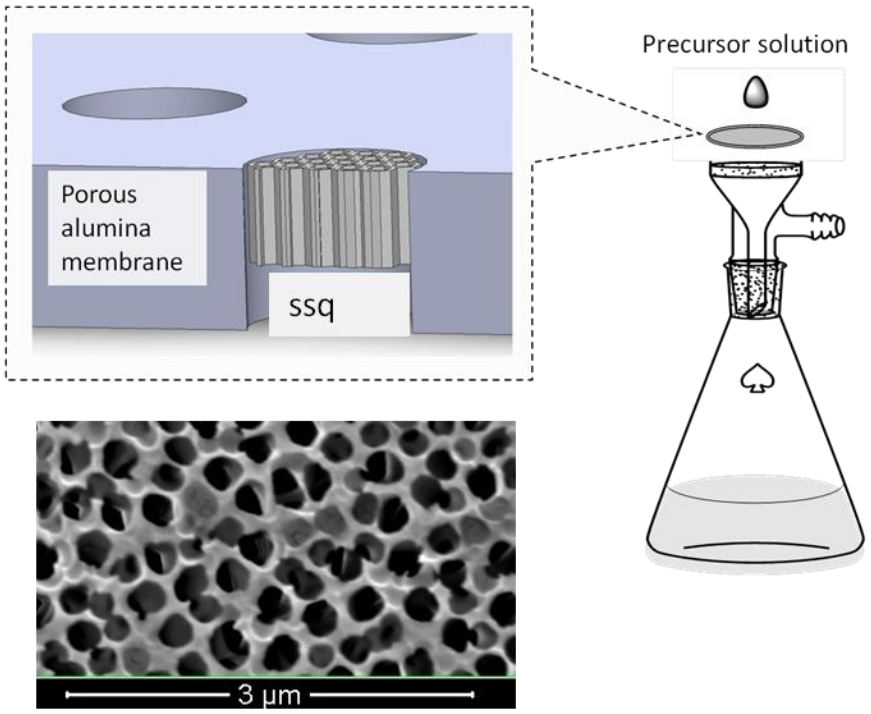

Figure 4.1 Fabrication of a ssq membrane using an aspirator.

4.3.1.3 Gold nanoparticle (AuNP) synthesis

AuNPs capped with dodecanethiol were synthesized by the revised Stucky method.[19] Briefly, 10 µL of dodecanethiol was added to 1 mL of a 40 mM $AuClPPh_3$ solution in benzene, followed by the addition of an equal volume of 115 mM borane-*tert*-butylamine complex. The mixture was placed in a silicon oil bath at room temperature, 55 ˚C or 100˚C to generate 2 nm, 6 nm, or 8 nm AuNPs, respectively, and was stirred until the clear and colorless mixture turned brown and eventually become a dark red solution. This colloidal mixture solution was mixed with an equal volume of ethanol and centrifuged. The supernatant was removed. A black power was collected after the

evaporation of the remaining solvent using a stream of nitrogen gas. Particle size and UV-Vis-NIR data were obtained by transmission electron microscopy (TEM) and UV-Vis-NIR spectrophotometry.

4.3.2 Filtration test

AuNPs and macromolecules were filtered on a custom-made dead-end filtration device. A 5 mL aliquot of the gold solution in chloroform was applied to the ssq membrane and filtered under gentle vacuum. Each feed and permeate solution was collected and was studied by monitoring the change in particle size distribution using transmission electron microscopy (TEM). The macromolecule solution in MES buffer was placed in feed vials and pressurized with 5 psi of N_2. The permeate solution was collected from the portion passing through the membrane, and the retentate was collected on the membrane surface. The macromolecule concentrations in the feed, retentate, and permeate were measured with a UV-Vis spectrometer (Agilent 8453, Santa Clara, CA, USA) using the absorption band at 281 nm for BSA and at 632 nm for myoglobin. The concentration of each retentate (C_R) and permeate (C_P) solution was used to calculate the rejection percentage (R%): $R=(1-C_P/C_R)*100\%$.

4.3.3 Analyses

The top surface and side morphologies of the ssq membrane were analyzed using a field-emission scanning electron microscope (Quanta 600F FEG SEM, FEI, Hillsboro, OR, USA) that operated at 30 kV. The ssq membrane samples were dried under vacuum and were sputter coated with gold using a vacuum electric sputter coater (Sputter Coater 108auto, Cressington, Watford, UK) before being mounted onto the

SEM sample holder for imaging. Scanning transmission electron microscopy (STEM) was accomplished using a Philips CM12 microscope with an accelerating voltage of 80 kV or 120 kV. For STEM, samples were dissolved in chloroform, added dropwise to a formvar-coated copper grid and then dried under vacuum. UV-Vis spectra were collected on an Agilent 8453.

4.4 Results and discussion

4.4.1 Morphology of the ssq membrane

The SEM images show bundles of ssq channels inside the AAM pores. (Figure 4.2A, B) The ssq nanotubes are aligned vertically on the membrane surface. Also, space was observed between the ssq nanotubes and the AAM membrane wall attributed to contraction during the drying and calcination process. This space is similar to that observed for silica nanotubes on AAMs. [20] After complete removal of the AAM, the ssq nanotubes were observed to be in regular and continuous alignment along the vertical axis. (Figure 4.2C, D)

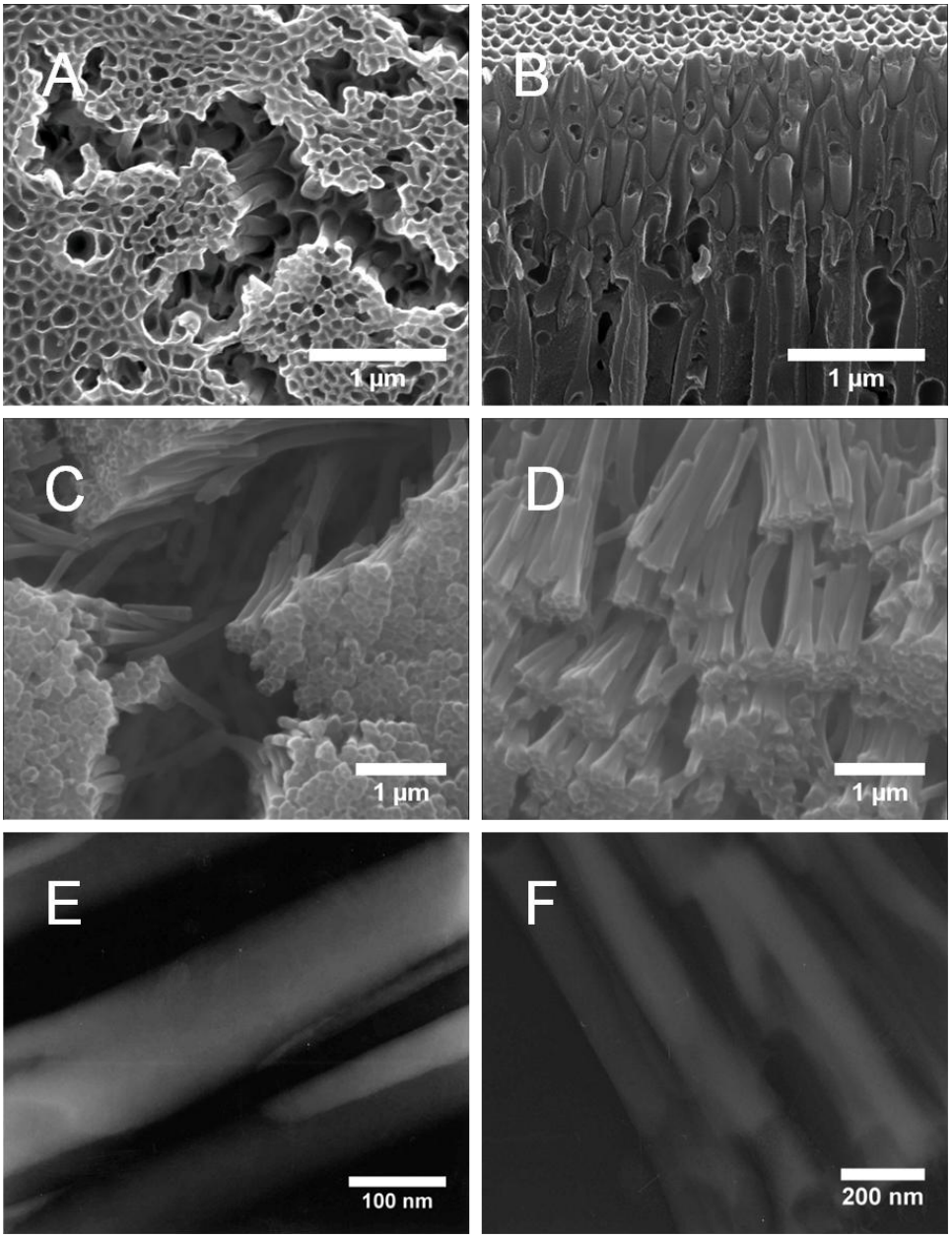

Figure 4.2 SEM plan-view (A) and cross section (B) images of the ssq membrane after partial etching of the alumina support with 8% H_3PO_4 for 270 min or 50 min, respectively. SEM plan-view (C), cross section (D) and TEM (E and F) images of ssq nanochannels were recorded after complete etching of the alumina matrix with 8% H_3PO_4 for 12 hr. SEM images (A and B) show evidence of the ssq nanochannels inside of the anodic alumina membrane. The ssq nanochannels (C and D) are uniform and are continuously aligned along the perpendicular (flow) axis.

4.4.2 Separation and purification of gold nanoparticles using the ssq membrane

The ssq membrane was evaluated using 5-8 nm gold nanoparticles protected with dodecanethiol. A 5 mL aliquot of a gold nanoparticle solution in chloroform was applied to the ssq membrane and filtered under gentle vacuum. Each feed and permeate solution was studied by monitoring the change in particle size distribution using transmission electron microscopy (TEM) following filtration. The feed solution histogram (3A') shows a wide particle size distribution (between 5 and 8 nm) for an unfiltered initial sample, while the permeate (3B') exhibits a particle size of 4.4 ± 0.6 nm, which is an impressively narrow particle size distribution. (Figure 4.3) PbS (oleic acid) nanoparticles (3.5 ± 0.8 nm, λmax = 1200 nm, plus aggregates) were also filtered using the ssq membrane. After filtration, a particle size of 3.5 ± 0.7 nm was determined by TEM analysis, which confirmed that the smaller particles (< 5 nm) were passing through the ssq membrane while the larger aggregates were being retained. These results indicate that the ssq membrane possessed the desired 5 nm cut-off.

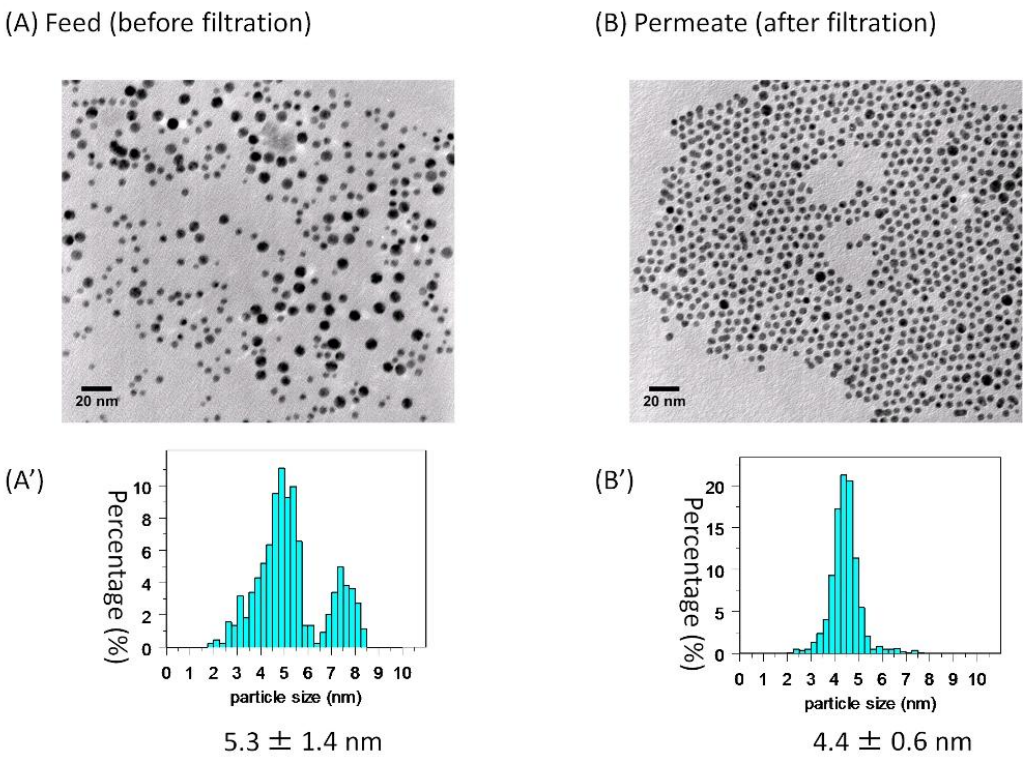

Figure 4.3 TEM images and particle size histograms of the feed solution (A) and the permeate solution (B) of gold nanoparticle mixtures filtered using the ssq membrane.

4.4.3 Ssq membrane performance metrics for macromolecules

A feed volume of 20 mL of each solution (0.2 mM myoglobin and 0.05 mM bovine serum albumin in 100 mM 2-(N-morpholino)ethanesulfonic buffer) was subjected to filtration separately on a similarly prepared ssq membrane at 40 psi by dead-end flow filtration. The hydrodynamic size of BSA and myoglobin are ~7.2 nm and ~3.2 nm, respectively. [21] An untreated AAM showed no separation of BSA or myoglobin. [16,22] Rejection values for myoglobin and BSA on the ssq membrane were experimentally determined to be 31.8% and 97.4%, respectively. (Figure 4.4) These results agree with the results previously obtained using gold nanoparticles on similarly

prepared ssq membranes, (section 4.4.2) where separation of nanoparticles smaller than 5 nm was successfully accomplished. BSA (larger particles larger than the 5 nm size of the ssq pores) was retained, while myoglobin being smaller than 5 nm, demonstrated the expected low rejection and passed through the ssq membrane.

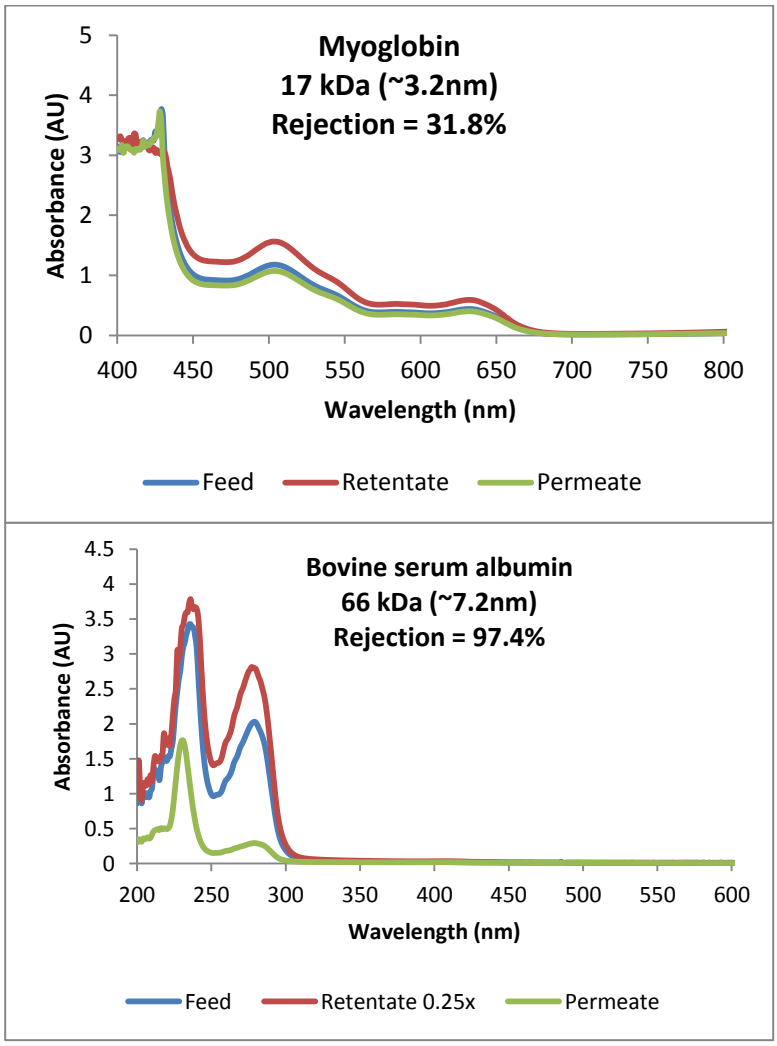

Figure 4.4 UV-Vis absorbance spectra of the feed, retentate, and permeate solutions of each Myoglobin and bovine serum albumin solution after filtration. Each macromolecular solution was subjected to the ssq membrane at 40 psi of N_2 gas pressure and ambient conditions.

4.5 Conclusion

Silsesquioxanes (ssq) can be utilized as nanochannels inside the pores of an AAM. The ssq nanochannels are mostly parallel to the AAM pore direction and can be used to give the membrane a smaller effective pore size. The ssq membrane was successfully employed for the separation of nanoparticles and macromolecules in non-aqueous and aqueous systems. The estimated cut-off of the ssq membrane is ~5 nm. We expect that the ssq membrane can be used with the AAM as a nanochannel microfluidic device. [23,24]

4.6 References

[1] Jan C. T. Eijkel, Albert van den Berg, Lab Chip 6 (2006) 19-23.

[2] A. Saxena, B.P. Tripathi, M. Kumar, V.K. Shahi, Adv. Colloid Interface Sci. 145 (2009) 1-22.

[3] Y. Yamauchi, N. Suzuki, T. Kimura, Chem. Commun. (2009) 5689.

[4] N. Suzuki, Y. Yamauchi, J. Nanomater. 2010 (2010) 1-4.

[5] N. Suzuki, T. Kimura, Y. Yamauchi, J. Mater. Chem. 20 (2010) 5294.

[6] Y. Piao, H. Kim, J. Nanosci. Nanotech. 9 (2009) 2215-2233.

[7] B. Platschek, A. Keilbach, T. Bein, Adv. Mater. (2011).

[8] S.A. El-Safty, TrAC, Trends Anal. Chem 30 (2011) 447-458.

[9] M. Meireles, A. Bessieres, I. Rogissart, P. Aimar, V. Sanchez, J. Membr. Sci. 103 (1995) 105-115.

[10] Y.H. See Toh, X.X. Loh, K. Li, A. Bismarck, A.G. Livingston, J. Membr. Sci. 291 (2007) 120-125.

[11] N.N. Li, A.G. Fane, W.S.W. Ho, T. Matsuura, in:, Advanced Membrane Technology and Applications, 1st ed., Wiley-AIChE, 2008, pp. 101-129.

[12] P. Aimar, M. Meireles, J. Membr. Sci. 346 (2010) 233-239.

[13] H. Susanto, M. Ulbricht, in:, Membrane Operations: Innovative Separations and Transformations, Wiley-VCH, 2009, pp. 19-43.

[14] F. Hoffmann, M. Cornelius, J. Morell, M. Fröba, Angew. Chem. Int. Ed. 45 (2006) 3216-3251.

[15] F. Hoffmann, M. Fröba, in:, The Supramolecular Chemistry of Organic-Inorganic Hybrid Materials, 2010, pp. 37-111.

[16] A. Yamaguchi, F. Uejo, T. Yoda, T. Uchida, Y. Tanamura, T. Yamashita, N. Teramae, Nat. Mater. 3 (2004) 337-341.

[17] P. Braunstein, H. Lehner, D. Matt, Inorg. Synth. 27 (1990) 218-221.

[18] A. Keilbach, M. Döblinger, R. Köhn, H. Amenitsch, T. Bein, Chem. Eur. J. 15 (2009) 6645-6650.

[19] N. Zheng, J. Fan, G.D. Stucky, J. Am. Chem. Soc. 128 (2006) 6550-6551.

[20] K. Jin, B. Yao, N. Wang, Chem. Phys. Lett. 409 (2005) 172-176.

[21] M.T. Tyn, T.W. Gusek, Biotechnol. Bioeng. 35 (1990) 327-338.

[22] H.U. Osmanbeyoglu, T.B. Hur, H.K. Kim, J. Membr. Sci. 343 (2009) 1-6.

[23] T. Sano, N. Iguchi, K. Iida, T. Sakamoto, M. Baba, H. Kawaura, Appl. Phys. Lett. 83 (2003) 4438.

[24] T. Yamashita, S. Kodama, T. Kemmei, M. Ohto, E. Nakayama, T. Muramoto, A. Yamaguchi, N. Teramae, N. Takayanagi, Lab Chip 9 (2009) 1337-1339.

Chapter 5 Conclusion

Organic-solvent resistant nanofiltration and ultrafiltration membranes were applied to the purification and separation of nanoparticles using a macroscale test fixture and a microextractor. The post-synthetic gold eleven nanoparticles (Au_{11}), the smallest cluster studied, was subjected to nanofiltration using various membranes, whose small pore size successfully retained the nanoparticles while passing byproducts such as unreacted precursors and ligands. The microextractor was shown to facilitate membrane maintenance and in-line connection with a synthesis part with an upstream synthetic reactor. The microextractor, coupled with the microreactor, was applied for continuous diafiltration which was shown to enhance and extend membrane performance and efficiency. In addition, nanofiltration was shown to generate less organic waste and was more rapid and "greener" than conventional purification methods. Future work includes the use of polymeric nanofiltration membranes in microfluidic devices for fractionation and concentration of nanoparticles for the purposes of catalysis or optical labeling.

2-8 nm organic-soluble gold and lead sulfide nanoparticles were purified and separated using commercially available organic-solvent resistant nanofiltration and ultrafiltration membranes in a home built device. The smaller pore size of the nanofiltration membrane provided for high rejection values (R>95%) of 2-8 nm gold and lead sulfide nanoparticles using retention of nanoparticles and removal of byproducts. The ultrafiltration membranes, HFM-100 and MPF-U20S, were also used

for size-fractionation of PbS and gold nanoparticles. HFM-100 and MPF-U20S demonstrated different rejection performance from similar size ranges of PbS nanoparticles and gold nanoparticles. Differences in the passivation layer, (PbS nanoparticles and gold nanoparticles were oleic acid and dodecanethiol, respectively) may in part be responsible for the different interactions with membrane materials and solvents. Future plans include successive nanoparticle recycling and extraction of an organic solvent using the ultrafiltration and nanofiltration membranes in a single module.

The integration of silsesquioxane (ssq) into macropores of an Anodisc alumina membrane (AAM) was shown to provide the mesopores for the separation of nanoparticles and macromolecules. The hard template of the AAM is suitable for weakly acidic or weakly basic ssq synthesis conditions. The ssq membrane was able to separate non-aqueous and aqueous nanomaterials, providing a ~5nm estimated cut-off. Future research is included that the ssq integration in microfluidic channels is able to concentration and filtration of nanoparticles and macromolecules from in-line microreactor synthesis. Extensive variation of silsesquioxane synthesis conditions such as variation of precursor, solvent, and surfactant concentration, curing temperature and time will be able to fabricate the different pore size of ssq membranes.

Bibliography

[1] M. C. Roco, National Nanotechnology Investment in the FY 2012 Budget, in: AAAS REPORT XXXVI - RESEARCH AND DEVELOPMENT FY 2012, American Association for the Advancement of Science, 2011.

[2] G. Cao, Nanostructures & Nanomaterials: Synthesis, Properties & Applications, 1st ed., Imperial College Press, 2004.

[3] R. Boistelle, J.P. Astier, Crystallization mechanisms in solution, J. Cryst. Growth. 90 (1988) 14-30.

[4] F.-K. Liu, Analysis and applications of nanoparticles in the separation sciences: A case of gold nanoparticles, J. Chromatogr. A. 1216 (2009) 9034-9047.

[5] L. Yu, A. Andriola, Quantitative gold nanoparticle analysis methods: A review, Talanta. 82 (2010) 869-875.

[6] L. Cademartiri, G.A. Ozin, Concepts of Nanochemistry, Wiley-VCH, 2009.

[7] C.B. Murray, D.J. Norris, M.G. Bawendi, Synthesis and characterization of nearly monodisperse CdE (E = sulfur, selenium, tellurium) semiconductor nanocrystallites, J. Am. Chem. Soc. 115 (1993) 8706-8715.

[8] J.P. Novak, C. Nickerson, S. Franzen, D.L. Feldheim, Purification of Molecularly Bridged Metal Nanoparticle Arrays by Centrifugation and Size Exclusion Chromatography, Anal. Chem. 73 (2001) 5758-5761.

[9] X. Sun, S.M. Tabakman, W. Seo, L. Zhang, G. Zhang, S. Sherlock, et al., Separation of Nanoparticles in a Density Gradient: FeCo@C and Gold Nanocrystals, Angew. Chem. Int. Ed. 48 (2009) 939-942.

[10] L. Bai, X. Ma, J. Liu, X. Sun, D. Zhao, D.G. Evans, Rapid Separation and Purification of Nanoparticles in Organic Density Gradients, J. Am. Chem. Soc. 132 (2010) 2333-2337.

[11] D. Steinigeweg, M. Schütz, M. Salehi, S. Schlücker, Fast and Cost- Effective Purification of Gold Nanoparticles in the 20–250 nm Size Range by Continuous Density Gradient Centrifugation, Small. (2011).

[12] B. Xiong, J. Cheng, Y. Qiao, R. Zhou, Y. He, E.S. Yeung, Separation of nanorods by density gradient centrifugation, J. Chromatogr. A. 1218 (2011) 3823-3829.

[13] A. Saxena, B.P. Tripathi, M. Kumar, V.K. Shahi, Membrane-based techniques for the separation and purification of proteins: An overview, Adv. Colloid Interface Sci. 145 (2009) 1-22.

[14] W. J. Koros, Y. H. Ma, T. Shimidzu, Terminology for membranes and membrane processes (IUPAC Recommendation 1996), J. Membr. Sci. 120 (1996) 149-159.

[15] Q.-L. Xie, J. Liu, X.-X. Xu, G.-B. Han, H.-P. Xia, X.-M. He, Size separation of Fe2O3 nanoparticles via membrane processing, Sep. Purif. Technol. 66 (2009) 148-152.

[16] I. Arnaud, J.-P. Abid, C. Roussel, H.H. Girault, Size-selective separation of gold nanoparticles using isoelectric focusing electrophoresis (IEF), Chem. Commun. (2005) 787.

[17] S.F. Sweeney, G.H. Woehrle, J.E. Hutchison, Rapid Purification and Size Separation of Gold Nanoparticles via Diafiltration., J. Am. Chem. Soc. 128 (2006) 3190-3197.

[18] J.C. Trefry, J.L. Monahan, K.M. Weaver, A.J. Meyerhoefer, M.M. Markopolous, Z.S. Arnold, et al., Size Selection and Concentration of Silver Nanoparticles by Tangential Flow Ultrafiltration for SERS-Based Biosensors, J. Am. Chem. Soc. 132 (2010) 10970-10972.

[19] D. Jassby, S.-R. Chae, Z. Hendren, M. Wiesner, Membrane filtration of fullerene nanoparticle suspensions: Effects of derivatization, pressure, electrolyte species and concentration, J. Colloid Interface Sci. 346 (2010) 296-302.

[20] K.C. Pradel, K. Sohn, J. Huang, Cross- Flow Purification of Nanowires, Angew. Chem. Int. Ed. 50 (2011) 3412-3416.

[21] P. Vandezande, L.E.M. Gevers, I.F.J. Vankelecom, Solvent resistant nanofiltration: separating on a molecular level, Chem. Soc. Rev. 37 (2008) 365-405.

[22] B. Zhao, H. Hu, S. Niyogi, M.E. Itkis, M.A. Hamon, P. Bhowmik, et al., Chromatographic Purification and Properties of Soluble Single-Walled Carbon Nanotubes, J. Am. Chem. Soc. 123 (2001) 11673-11677.

[23] S. Niyogi, H. Hu, M.A. Hamon, P. Bhowmik, B. Zhao, S.M. Rozenzhak, et al., Chromatographic Purification of Soluble Single-Walled Carbon Nanotubes (s-SWNTs), J. Am. Chem. Soc. 123 (2001) 733-734.

[24] D. Chattopadhyay, S. Lastella, S. Kim, F. Papadimitrakopoulos, Length Separation of Zwitterion-Functionalized Single Wall Carbon Nanotubes by GPC, J. Am. Chem. Soc. 124 (2002) 728-729.

[25] X. Xu, R. Ray, Y. Gu, H.J. Ploehn, L. Gearheart, K. Raker, et al., Electrophoretic Analysis and Purification of Fluorescent Single-Walled Carbon Nanotube Fragments, J. Am. Chem. Soc. 126 (2004) 12736-12737.

[26] K.M. Krueger, A.M. Al-Somali, J.C. Falkner, V.L. Colvin, Characterization of Nanocrystalline CdSe by Size Exclusion Chromatography, Anal. Chem. 77 (2005) 3511-3515.

[27] K. Sakai-Kato, S. Ota, T. Takeuchi, T. Kawanishi, Size separation of colloidally dispersed nanoparticles using a monolithic capillary column, J. Chromatogr. A. 1218 (2011) 5520-5526.

[28] G.-T. Wei, F.-K. Liu, Separation of nanometer gold particles by size exclusion chromatography, J. Chromatogr. A. 836 (1999) 253-260.

[29] G.-T. Wei, F.-K. Liu, C.R.C. Wang, Shape Separation of Nanometer Gold Particles by Size-Exclusion Chromatography, Anal. Chem. 71 (1999) 2085-2091.

[30] A.M. Al-Somali, K.M. Krueger, J.C. Falkner, V.L. Colvin, Recycling Size Exclusion Chromatography for the Analysis and Separation of Nanocrystalline Gold, Anal. Chem. 76 (2004) 5903-5910.

[31] J.P. Wilcoxon, P. Provencio, Etching and Aging Effects in Nanosize Au Clusters Investigated Using High-Resolution Size-Exclusion Chromatography, J. Phys. Chem. B. 107 (2003) 12949-12957.

[32] J.P. Wilcoxon, J.E. Martin, P. Provencio, Size Distributions of Gold Nanoclusters Studied by Liquid Chromatography, Langmuir. 16 (2000) 9912-9920.

[33] H. Tsunoyama, Y. Negishi, T. Tsukuda, Chromatographic Isolation of "Missing" Au55 Clusters Protected by Alkanethiolates, J. Am. Chem. Soc. 128 (2006) 6036-6037.

[34] S. Knoppe, J. Boudon, I. Dolamic, A. Dass, T. Bu□rgi, Size Exclusion Chromatography for Semipreparative Scale Separation of Au38(SR)24 and Au40(SR)24 and Larger Clusters, Anal. Chem. 83 (2011) 5056-5061.

[35] V.L. Jimenez, M.C. Leopold, C. Mazzitelli, J.W. Jorgenson, R.W. Murray, HPLC of Monolayer-Protected Gold Nanoclusters, Anal. Chem. 75 (2003) 199-206.

[36] Y. Song, M.L. Heien, V. Jimenez, R.M. Wightman, R.W. Murray, Voltammetric Detection of Metal Nanoparticles Separated by Liquid Chromatography, Anal. Chem. 76 (2004) 4911-4919.

[37] Y. Song, V. Jimenez, C. McKinney, R. Donkers, R.W. Murray, Estimation of Size for 1−2 nm Nanoparticles Using an HPLC Electrochemical Detector of Double Layer Charging, Anal. Chem. 75 (2003) 5088-5096.

[38] A. Dass, R. Guo, J.B. Tracy, R. Balasubramanian, A.D. Douglas, R.W. Murray, Gold Nanoparticles with Perfluorothiolate Ligands, Langmuir. 24 (2008) 310-315.

[39] R.L. Wolfe, R.W. Murray, Analytical Evidence for the Monolayer-Protected Cluster Au225[(S(CH2)5CH3)]75, Anal. Chem. 78 (2006) 1167-1173.

[40] M. Hanauer, S. Pierrat, I. Zins, A. Lotz, C. Sönnichsen, Separation of Nanoparticles by Gel Electrophoresis According to Size and Shape, Nano Letters. 7 (2007) 2881-2885.

[41] A.I. López-Lorente, B.M. Simonet, M. Valcárcel, Electrophoretic methods for the analysis of nanoparticles, TrAC, Trends Anal. Chem. 30 (2011) 58-71.

[42] F. von der Kammer, S. Legros, T. Hofmann, E.H. Larsen, K. Loeschner, Separation and characterization of nanoparticles in complex food and environmental samples by field-flow fractionation, TrAC, Trends Anal. Chem. 30 (2011) 425-436.

[43] G.L. Hornyak, S. Peschel, T. Sawitowski, G. Schmid, TEM, STM and AFM as tools to study clusters and colloids, Micron. 29 (1998) 183-190.

[44] W.D. Pyrz, D.J. Buttrey, Particle Size Determination Using TEM: A Discussion of Image Acquisition and Analysis for the Novice Microscopist, Langmuir. 24 (2008) 11350-11360.

[45] P. Mulvaney, Surface Plasmon Spectroscopy of Nanosized Metal Particles, Langmuir. 12 (1996) 788-800.

[46] F. Hoffmann, M. Cornelius, J. Morell, M. Fröba, Silica-Based Mesoporous Organic–Inorganic Hybrid Materials, Angew. Chem. Int. Ed. 45 (2006) 3216-3251.

[47] Ö. Dag, C. Yoshina- Ishii, T. Asefa, M.J. MacLachlan, H. Grondey, N. Coombs, et al., Oriented Periodic Mesoporous Organosilica (PMO) Film with Organic Functionality Inside the Channel Walls, Adv. Funct. Mater. 11 (2001) 213-217.

[48] G. Schottner, Hybrid Sol−Gel-Derived Polymers: Applications of Multifunctional Materials, Chem. Mater. 13 (2001) 3422-3435.

[49] W.J. Hunks, G.A. Ozin, Challenges and advances in the chemistry of periodic mesoporous organosilicas (PMOs), J. Mater. Chem. 15 (2005) 3716-3724.

[50] Y. Lu, R. Ganguli, C.A. Drewien, M.T. Anderson, C.J. Brinker, W. Gong, et al., Continuous formation of supported cubic and hexagonal mesoporous films by sol-gel dip-coating, Nature. 389 (1997) 364-368.

[51] B.D. Hatton, K. Landskron, W. Whitnall, D.D. Perovic, G.A. Ozin, Spin-Coated Periodic Mesoporous Organosilica Thin Films - Towards a New Generation of Low-Dielectric-Constant Materials, Adv. Funct. Mater. 15 (2005) 823-829.

[52] G.J.A.A. Soler-Illia, P. Innocenzi, Mesoporous Hybrid Thin Films: The Physics and Chemistry Beneath, Chem. Eur. J. 12 (2006) 4478-4494.

[53] S.S. Park, C.-S. Ha, Free-Standing and Oriented Periodic Mesoporous Organosilica Films with Variable Pore Size at the Air−Water Interface, Chem. Mater. 17 (2005) 3519-3523.

[54] C.J. Brinker, Y. Lu, A. Sellinger, H. Fan, Evaporation-Induced Self-Assembly: Nanostructures Made Easy, Adv. Mater. 11 (1999) 579-585.

[55] Y. Lu, H. Fan, N. Doke, D.A. Loy, R.A. Assink, D.A. LaVan, et al., Evaporation-Induced Self-Assembly of Hybrid Bridged Silsesquioxane Film and Particulate Mesophases with Integral Organic Functionality, J. Am. Chem. Soc. 122 (2000) 5258-5261.

[56] A. Yamaguchi, F. Uejo, T. Yoda, T. Uchida, Y. Tanamura, T. Yamashita, et al., Self-assembly of a silica-surfactant nanocomposite in a porous alumina membrane, Nat. Mater. 3 (2004) 337-341.

[57] Y.-B. Jiang, G. Xomeritakis, Z. Chen, D. Dunphy, D.J. Kissel, J.L. Cecchi, et al., Sub-10 nm Thick Microporous Membranes Made by Plasma-Defined Atomic

Layer Deposition of a Bridged Silsesquioxane Precursor, J. Am. Chem. Soc. 129 (2007) 15446-15447.

[58] A.G.F. I, A. Schaefer, T.D. Waite, Nanofiltration: Principles and Applications, 1st ed., Elsevier Science, 2005.

[59] J.P. Sheth, Y. Qin, K.K. Sirkar, B.C. Baltzis, Nanofiltration-based diafiltration process for solvent exchange in pharmaceutical manufacturing, J. Membr. Sci. 211 (2003) 251-261.

[60] I. Sereewatthanawut, F.W. Lim, Y.S. Bhole, D. Ormerod, A. Horvath, A.T. Boam, et al., Demonstration of Molecular Purification in Polar Aprotic Solvents by Organic Solvent Nanofiltration, Org. Process Res. Dev. (2010).

[61] S. So, L.G. Peeva, E.W. Tate, R.J. Leatherbarrow, A.G. Livingston, Organic Solvent Nanofiltration: A New Paradigm in Peptide Synthesis, Org. Process Res. Dev. 14 (2010) 1313-1325.

[62] C. Van Doorslaer, D. Glas, A. Peeters, A. Cano Odena, I. Vankelecom, K. Binnemans, et al., Product recovery from ionic liquids by solvent-resistant nanofiltration: application to ozonation of acetals and methyl oleate, Green Chem. 12 (2010) 1726.

[63] G.H. Woehrle, L.O. Brown, J.E. Hutchison, Thiol-Functionalized, 1.5-nm Gold Nanoparticles through Ligand Exchange Reactions: Scope and Mechanism of Ligand Exchange, J. Am. Chem. Soc. 127 (2005) 2172-2183.

[64] G.H. Woehrle, M.G. Warner, J.E. Hutchison, Molecular-Level Control of Feature Separation in One-Dimensional Nanostructure Assemblies Formed by Biomolecular Nanolithography, Langmuir. 20 (2004) 5982-5988.

[65] G.H. Woehrle, M.G. Warner, J.E. Hutchison, Ligand Exchange Reactions Yield Subnanometer, Thiol-Stabilized Gold Particles with Defined Optical Transitions, J. Phys. Chem. B. 106 (2002) 9979-9981.

[66] L.C. McKenzie, Mechanistic insights on nanoparticle formation: investigation of reaction pathways and development of controlled syntheses for triphenylphosphine-stabilized undecagold, PhD Dissertation, University of Oregon, 2009.

[67] J.P. Novak, C. Nickerson, S. Franzen, D.L. Feldheim, Purification of Molecularly Bridged Metal Nanoparticle Arrays by Centrifugation and Size Exclusion Chromatography, Anal. Chem. 73 (2001) 5758-5761.

[68] C. Contado, R. Argazzi, Size sorting of citrate reduced gold nanoparticles by sedimentation field-flow fractionation., J. Chromatogr. A. 1216 (2009) 9088-9098.

[69] A. Akthakul, A.I. Hochbaum, F. Stellacci, A.M. Mayes, Size Fractionation of Metal Nanoparticles by Membrane Filtration, Adv. Mater. 17 (2005) 532-535.

[70] Y. Liu, H. Tsunoyama, T. Akita, T. Tsukuda, Preparation of ~1 nm Gold Clusters Confined within Mesoporous Silica and Microwave-Assisted Catalytic Application for Alcohol Oxidation, J. Phys. Chem. C. 113 (2009) 13457-13461.

[71] S. Ariyasu, A. Onoda, R. Sakamoto, T. Yamamura, Conjugation of Au11 cluster with Cys-rich peptides containing the α-domain of metallothionein, Dalton Trans. (2009) 3742.

[72] Y. Shichibu, Y. Negishi, T. Tsukuda, T. Teranishi, Large-Scale Synthesis of Thiolated Au25 Clusters via Ligand Exchange Reactions of Phosphine-Stabilized Au11 Clusters, J. Am. Chem. Soc. 127 (2005) 13464-13465.

[73] A. Buekenhoudt, M. Reyes, M. dez Miguel, Stability of Porous Ceramic Membranes, in: Inorganic Membranes: Synthesis, Characterization and Applications, Elsevier, 2008: pp. 1-31.

[74] K. Li, Ceramic membranes for separation and reaction, John Wiley and Sons, 2007.

[75] T. Kim, G.K. Lingam, B.K. Paul, V.T. Remcho, On-line, continuous nanofiltration of gold eleven nanoparticles (Au_{11}) produced synthetically in a microreactor, in: MicroTas2009, The Chemical and Biological Microsystems Society, Jeju, South Korea, 2009: pp. 1210-1212.

[76] P. Braunstein, H. Lehner, D. Matt, A Platinum-Gold Cluster: Chloro-1κCl-Bis(Triethylphosphine-1κP)Bis(Triphenyl- Phosphine)-2κP, 3κP-Triangulo- Digold-Platinum(1 +) Trifluoromethanesulfonate, Inorg. Synth. 27 (1990) 218-221.

[77] J.T. Rundel, B.K. Paul, V.T. Remcho, Organic solvent nanofiltration for microfluidic purification of poly(amidoamine) dendrimers, J. Chromatogr. A. 1162 (2007) 167-174.

[78] Hyung Dae Jin, A. Garrison, T. Tseng, B.K. Paul, Chih-Hung Chang, High-rate synthesis of phosphine-stabilized undecagold nanoclusters using a multilayered micromixer, Nanotechnology. 21 (2010) 445604.

[79] G.H. Woehrle, J.E. Hutchison, Thiol-Functionalized Undecagold Clusters by Ligand Exchange: Synthesis, Mechanism, and Properties, Inorg. Chem. 44 (2005) 6149-6158.

[80] W. Koschuh, V.H. Thang, S. Krasteva, S. Novalin, K.D. Kulbe, Flux and retention behaviour of nanofiltration and fine ultrafiltration membranes in filtrating juice from a green biorefinery: A membrane screening, J. Membr. Sci. 261 (2005) 121-128.

[81] M.A. Hines, G.D. Scholes, Colloidal PbS Nanocrystals with Size-Tunable Near-Infrared Emission: Observation of Post-Synthesis Self-Narrowing of the Particle Size Distribution, Adv. Mater. 15 (2003) 1844-1849.

[82] A.L. Rogach, A. Eychmüller, S.G. Hickey, S.V. Kershaw, Infrared-Emitting Colloidal Nanocrystals: Synthesis, Assembly, Spectroscopy, and Applications, Small. 3 (2007) 536-557.

[83] I. Moreels, K. Lambert, D. Smeets, D. De Muynck, T. Nollet, J.C. Martins, et al., Size-Dependent Optical Properties of Colloidal PbS Quantum Dots, ACS Nano. 3 (2009) 3023-3030.

[84] X. Gao, Y. Cui, R.M. Levenson, L.W.K. Chung, S. Nie, In vivo cancer targeting and imaging with semiconductor quantum dots, Nat. Biotech. 22 (2004) 969-976.

[85] H. Li, D. Chen, L. Li, F. Tang, L. Zhang, J. Ren, Size- and shape-controlled synthesis of PbSe and PbS nanocrystals via a facile method, CrystEngComm. 12 (2010) 1127.

[86] T.-Y. Liu, M. Li, J. Ouyang, M.B. Zaman, R. Wang, X. Wu, et al., Non-Injection and Low-Temperature Approach to Colloidal Photoluminescent PbS Nanocrystals with Narrow Bandwidth, J. Phys. Chem. C. 113 (2009) 2301-2308.

[87] A. Chemseddine, H. Weller, Highly monodisperse quantum sized cadmium sulfide particles by size selective precipitation., Ber. Bunsen-Ges. Phys. Chem. 97 (1993) 636-7.

[88] T. Siebrands, M. Giersig, P. Mulvaney, C.H. Fischer, Steric exclusion chromatography of nanometer-sized gold particles, Langmuir. 9 (1993) 2297-2300.

[89] S. Knoppe, J. Boudon, I. Dolamic, A. Dass, T. Bürgi, Size Exclusion Chromatography for Semipreparative Scale Separation of Au38(SR)24 and Au40(SR)24 and Larger Clusters, Anal. Chem. 0 (2011).

[90] I. Limayem, C. Charcosset, H. Fessi, Purification of nanoparticle suspensions by a concentration/diafiltration process, Sep. Purif. Technol. 38 (2004) 1-9.

[91] B. Vanderbruggen, M. Manttari, M. Nystrom, Drawbacks of applying nanofiltration and how to avoid them: A review, Sep. Purif. Technol. 63 (2008) 251-263.

[92] H. Kim, S. Nakai, Simple Separation of Immunoglobulin from Egg Yolk by Ultrafiltration, J. Food Sci. 63 (1998) 485-490.

[93] H.K. Shon, S.H. Kim, S. Vigneswaran, R. Ben Aim, S. Lee, J. Cho, Physicochemical pretreatment of seawater: fouling reduction and membrane characterization, Desalination. 238 (2009) 10-21.

[94] C. Pagliero, N. Ochoa, J. Marchese, M. Mattea, Degumming of crude soybean oil by ultrafiltration using polymeric membranes, J. Am. Oil Chem. Soc. 78 (2001) 793-796.

[95] N. Zheng, J. Fan, G.D. Stucky, One-Step One-Phase Synthesis of Monodisperse Noble-Metallic Nanoparticles and Their Colloidal Crystals, J. Am. Chem. Soc. 128 (2006) 6550-6551.

[96] Image J 1.42. This is a shareware image processing program. rsbweb.nib.gov/ij/download.html, n.d.

[97] G.D. Scholes, Controlling the Optical Properties of Inorganic Nanoparticles, Adv. Funct. Mater. 18 (2008) 1157-1172.

[98] S. Darvishmanesh, J. Degrève, B. Van der Bruggen, Mechanisms of solute rejection in solvent resistant nanofiltration: the effect of solvent on solute rejection, Phys. Chem. Chem. Phys. 12 (2010) 13333.

[99] R. Shukla, M. Cheryan, Performance of ultrafiltration membranes in ethanol-water solutions: effect of membrane conditioning, J. Membr. Sci. 198 (2002) 75-85.

[100] Jan C. T. Eijkel, Albert van den Berg, Nanotechnology for membranes, filters and sieves A series of mini-reviews covering new trends in fundamental and applied

research, and potential applications of miniaturised technologies, Lab Chip. 6 (2006) 19-23.

[101] Y. Yamauchi, N. Suzuki, T. Kimura, Formation of mesoporous oxide fibers in polycarbonate confined spaces, Chem. Commun. (2009) 5689.

[102] N. Suzuki, Y. Yamauchi, Fabrication of Mesostructured Silica and Titania Rods on Substrates by Using Polycarbonate Membranes, J. Nanomater. 2010 (2010) 1-4.

[103] N. Suzuki, T. Kimura, Y. Yamauchi, General synthesis of fibrous mesoporous metal oxides in polycarbonate membrane, J. Mater. Chem. 20 (2010) 5294.

[104] Y. Piao, H. Kim, Fabrication of Nanostructured Materials Using Porous Alumina Template and Their Applications for Sensing and Electrocatalysis, J. Nanosci. Nanotech. 9 (2009) 2215-2233.

[105] B. Platschek, A. Keilbach, T. Bein, Mesoporous Structures Confined in Anodic Alumina Membranes, Adv. Mater. (2011).

[106] S.A. El-Safty, Designs for size-exclusion separation of macromolecules by densely-engineered mesofilters, TrAC, Trends Anal. Chem. 30 (2011) 447-458.

[107] M. Meireles, A. Bessieres, I. Rogissart, P. Aimar, V. Sanchez, An appropriate molecular size parameter for porous membranes calibration, J. Membr. Sci. 103 (1995) 105-115.

[108] Y.H. See Toh, X.X. Loh, K. Li, A. Bismarck, A.G. Livingston, In search of a standard method for the characterisation of organic solvent nanofiltration membranes, J. Membr. Sci. 291 (2007) 120-125.

[109] N.N. Li, A.G. Fane, W.S.W. Ho, T. Matsuura, Microfiltratoin and Ultrafiltration, in: Advanced Membrane Technology and Applications, 1st ed., Wiley-AIChE, 2008: pp. 101-129.

[110] P. Aimar, M. Meireles, Calibration of ultrafiltration membranes against size exclusion chromatography columns, J. Membr. Sci. 346 (2010) 233-239.

[111] H. Susanto, M. Ulbricht, Polymeric Membranes for Molecular Separations, in: Membrane Operations: Innovative Separations and Transformations, Wiley-VCH, 2009: pp. 19-43.

[112] F. Hoffmann, M. Fröba, Silica-Based Mesoporous Organic–Inorganic Hybrid Materials, in: The Supramolecular Chemistry of Organic-Inorganic Hybrid Materials, 2010: pp. 37-111.

[113] A. Keilbach, M. Döblinger, R. Köhn, H. Amenitsch, T. Bein, Periodic Mesoporous Organosilica in Confined Environments, Chem. Eur. J. 15 (2009) 6645-6650.

[114] K. Jin, B. Yao, N. Wang, Structural characterization of mesoporous silica nanowire arrays grown in porous alumina templates, Chem. Phys. Lett. 409 (2005) 172-176.

[115] M.T. Tyn, T.W. Gusek, Prediction of diffusion coefficients of proteins, Biotechnol. Bioeng. 35 (1990) 327-338.

[116] H.U. Osmanbeyoglu, T.B. Hur, H.K. Kim, Thin alumina nanoporous membranes for similar size biomolecule separation, J. Membr. Sci. 343 (2009) 1-6.

[117] T. Sano, N. Iguchi, K. Iida, T. Sakamoto, M. Baba, H. Kawaura, Size-exclusion chromatography using self-organized nanopores in anodic porous alumina, Appl. Phys. Lett. 83 (2003) 4438.

[118] T. Yamashita, S. Kodama, T. Kemmei, M. Ohto, E. Nakayama, T. Muramoto, et al., Separation of adenine, adenosine-5[prime or minute]-monophosphate and adenosine-5[prime or minute]-triphosphate by fluidic chip with nanometre-order diameter columns inside porous anodic alumina using an aqueous mobile phase, Lab Chip. 9 (2009) 1337-1339.